Turkish Journal of Earth Sciences (Turkish J. Earth Sci.), **Vol. 12**, 2003, pp. 215-239. *Copyright ©TÜBİTAK*

Mineralogy and Geochemistry of Melilite Leucitites, Balçıkhisar, Afyon (Turkey)

CÜNEYT AKAL

Dokuz Eylül Üniversitesi, Mühendislik Fakültesi, Jeoloji Mühendisliği Bölümü, TR-35100 Bornova, İzmir - Turkey
(e-mail: cuneyt.akal@deu.edu.tr)

Abstract: The Middle Miocene Afyon volcanic complex crops out in west-central Anatolia and comprises products of extensive potassic-ultrapotassic volcanic activity that intrude and/or cover the sedimentary formations of the western Taurides. Based on their stratigraphic setting, three stages of potassic and ultrapotassic volcanism are distinguishable. Melilite-leucitite lavas are the products of the first stage and followed by lamproites that represent the second stage of volcanism. The leucitite block- and fragment-rich Balçıkhisar volcaniclastic succession overlies the products of the first and second stage volcanism. Lacustrine sedimentary rocks cover the products of first and second stage volcanism. Lacustrine sedimentary rocks are gradationally overlain by the Tokluk volcano-sedimentary succession. Phonotephritic lava domes, dykes, and flows represent the third stage of volcanic activity.

Melilite leucitites from two occurrences in the Afyon volcanic province were studied. The melilite leucitites crop out as small lava domes and spatially limited lava flows. The melilite-leucitite lavas typically have porphyritic texture and are composed of leucite, nepheline, barium feldspar, melilite, diopside, melanite, calcite, apatite, and opaque minerals. Melilite crystals are relatively gehlenite- to akermanite-rich. The diopsidic clinopyroxene phenocrysts are partially and/or completely transformed to melilite aggregates.

Geochemically, the SiO_2 content of the melilite leucitites varies from 44% to 47% and they are ultrapotassic with K_2O contents of 9.5 to 11.8% and average Na_2O/K_2O of about 2. The Al_2O_3 and CaO contents are rather high (18%), whereas TiO_2 contents are low (1.22%). Melilite leucitites have highly fractionated REE and incompatible element compositions. The Ba (8745 ppm), Rb (670 ppm) and Sr (4802 ppm) contents are enriched relative to primitive mantle and chondrites. The melilite leucitites were generated by partial melting of a primitive mantle source or an enriched source near a subduction zone and collision processes related to an active plate margin.

Key Words: leucite, melilite, leucicite, ultrapotassic, Afyon volcanic region, west-central Anatolia

Melilit Lösititlerin Mineralojisi ve Jeokimyası, Balçıkhisar, Afyon (Türkiye)

Özet: Batı-Orta Anadolu'da yüzlek veren ve Batı Toroslar'a ait sedimanter formasyonları kesen ve/veya örten Orta Miyosen yaşlı Afyon volkanik kompleksi geniş yayılım sunan potasik-ultrapotasik aktivitenin ürünlerinden oluşmaktadır. Stratigrafik konumlarına dayalı olarak potasik ve ultrapotasik volkanizmanın üç evresi görülebilir. Melilit-lösitit lavları ilk evre volkanik faaliyetin ürünleridir. Lamproitler ise ikinci evre volkanik faaliyeti temsil etmektedirler. Lösitit blok ve parçalarınca zengin olan Balçıkhisar volkaniklasitik serisi birinci evre volkanik aktivitenin ürünlerini örtmektedir. Birinci ve ikinci evre volkanizmanın ürünleri gölsel sedimanter kayalar ile örtülmektedir. Bu gölsel sedimanter kayalar dereceli olarak Tokluk volkano-sedimanter serisi tarafından üstlenmektedir. Fonotefritik lav domları, daykları ve lav akmaları çalışma alanındaki üçüncü evre volkanik faaliyetleri oluşturmaktadır.

Afyon volkanik kompleksinde yeralan ve hacimsel olarak küçük lav domları ve lav akmaları şeklinde yüzlek veren iki melilit lösetit oluşumu çalışılmıştır. Tipik olarak porfiritik doku sunan melilit-lösitit lavları lösit, nefelin, baryum feldspat, melilit, diyopsid, melanit, kalsit, apatit ve opak minerallerden oluşmaktadır. Melilit kristallerinde genellikle gehlenit-akermanit bileşimi baskındır. Diopsid bileşimindeki klinopiroksen fenokristalleri kısmen ve/veya tamamen melilit tanelerine dönüşmüştür. Jeokimyasal olarak %9.5–11.8 arasındaki K_2O ve Na_2O/K_2O oranının ortalama 2 değerleri ile ultrapotasik karakterdeki melilit-lösititlerin SiO_2 bileşeni %44 ile %47 arasındadır. Al_2O_3 ve CaO bileşenleri %18 değerine ulaşırken ortalama TiO_2 bileşenleri %1.22 değerindedir. Melilit lösititler yüksek ayrımlaşma gösteren nadir toprak ve duraysız element bileşimlerine sahiptirler. Ba (8745 ppm), Rb (670 ppm) ve Sr (4802 ppm) bileşenleri ilksel manto ve kondritlere göre zenginleşmiştir. Melilit lösititler, dalma–batma ve çarpışma süreçlerinin geliştiği aktif kıta kenarına yakın ortamda kismi ergime ile meydana gelmiş ilksel bir eriğiyin üst kabuktan kısmen kirlenmesi ile oluşan bir magmanın ürünleridir.

Anahtar Sözcükler: lösit, melilit, lösitit, ultrapotasik, Afyon volkanik bölgesi, batı-orta Anadolu

Introduction

Potassic lavas have traditionally attracted scientific attention that is inversely proportional to their abundances. Prevalent interest in potassic rocks focuses on their unusual mineralogy, spectacular chemistry, mantle source compositions, and tectonic evolution of the lithosphere beneath potassic lava fields. Potassium-rich volcanic rocks are limited volumetrically but are widespread in several tectonic environments, such as intraplate rift zones in uplift areas or behind convergent plate margins and, to a lesser extent in oceanic intraplate settings. In the Mediterranean region, ultrapotassic rocks formed along the Alpine chain during the Neogene to Quaternary period. The most well-known potassic–ultrapotassic volcanic rocks are distributed near continental and convergent plate margins along the Alpine chain, and these include the Calatrava volcanic province of central Spain (Cebria & Lopez-Ruiz 1995), the Rhön area of Germany (Jung 1995), the Roman co-magmatic region (Beccaluva *et al.* 1991; Peccerillo 1992), and the Aeolian Islands (Clift & Blusztajn 1999) in Italy.

In Turkey, potassic to ultrapotassic volcanic rocks are located in the Afyon volcanic province, the Isparta area (Francalanci *et al.* 2000), and the Sivrihisar area (Özgenç 1993) (Figure 1). The rock suites from these areas share many characteristics and, in general, show that petrogenesis of potassic magma is not a singular event but must be related to an overall or general process or processes. The occurrence of potassium-rich volcanic rocks in the Afyon volcanic province (Turkey) has been known since the early 1970s (Keller & Villari 1972), but in spite of extensive studies by several researchers, there have been no recent mineralogical and stratigraphic examinations of these particular rocks.

Based on geochemical data from different localities in the Kırka-Afyon-Isparta volcanic areas, Francalanci *et al.* (1990, 2000) and Savaşçın *et al.* (1995) indicated that the rocks from the Kırka-Afyon area have an orogenic affinity, whereas those from the Isparta area exhibit orogenic and within-plate affinities. The ultrapotassic suite is a product of a residual, lithospheric mantle probably metasomatised by fluids and/or melts of different origin (subduction-related for Kırka-Afyon rocks; deep asthenospheric origin for Isparta rocks). A more fertile and probably deeper mantle, enriched by subduction-related components, was the source of the potassic rocks. Aydar *et al.* (1996) and Çoban *et al.* (2000) assumed that the ultrapotassic volcanic rocks were derived from a mantle enriched incompatible elements through mantle metasomatism.

Keller (1983) suggested that the Afyon volcanic area is a part of a Neogene volcanic belt, which follows the Tauride fold chains, related to Late Tertiary collision and subduction processes along the Cypriot-Taurus arc. Keller & Villari (1972) suggested that the main volcanic activity in the Afyon province developed at the Miocene–Pliocene boundary. In addition to these geodynamic interpretations, Besang *et al.* (1977) reported 10 K/Ar ages from highly potassic volcanic rocks of the southern part of Afyon region that ranges between 8.6 Ma and 14.75 Ma. The products of this Middle Miocene potassic-ultrapotassic volcanic activity overlie and intrude the sedimentary formations in the northeastern part of western Taurides, including the Geyik Dağ Unit and the Bozkır Unit (Özgül 1984). Geyik Dağ Unit is the autochthonous unit of the central Taurides and consists of platform-type sediments starting with a Lower Palaeozoic (Cambrian and Ordovician) basement rocks, followed by Mesozoic–Lower Tertiary rocks, made up largely of carbonates. The Bozkır Unit which, corresponds to the Beyşehir-Hoyran-Hadim Nappes of Poisson *et al.* (1984), comprises a mélange of pelagic sediment, spilite, diabase and ultramafic blocks of various sizes and ages; the age span of the blocks is between Late Triassic and Late Cretaceous. The Bozkır Unit tectonically overlies the Lutetian flysch of the Geyik Dağ Unit as a result of later Eocene movements (Özgül 1984). Detailed investigation and mapping of the sedimentary basement rocks, ranging in age from Triassic to Tertiary, was set forth by Öztürk & Öztürk (1989). That study showed that the northeastern most part of the western Taurides consists of a number of tectonostratigraphic rock groups with distinctive stratigraphical and structural features. As seen from the geological map, the Balçıkhisar Group and the Çölovası allochthonous units, which represent the basement rocks of the study area, were mapped and then compared and correlated with the classification of Öztürk & Öztürk (1989). Each group was simplified compared to those of Öztürk & Öztürk (1989).

The purpose of this paper is to present whole-rock major, trace and rare-earth element chemistry of the potassic suite and the mineral chemistries of the melilite leucitites, to determinate their geochemical affinities relative to probable sources and tectonic setting.

Geological Setting

Regional Tectonics

The northward subduction of the African Plate under Eurasia Plate resulted in an important continental collision that occurred during the Middle–Late Miocene (Fytikas *et al.* 1984). This collisional phase was followed by an extensional tectonic regime (Koçyiğit 1984; Savaşçın 1990; Savaşçın & Güleç 1990). The area located between the eastern part of western Anatolia and the western part of central Anatolia is dominated by complex structural elements (Figure 2). Koçyiğit (1984) indicated that several NE–SW- and NW–SE-trending cross-graben and horst structures bounded by active normal faults dominate the area between Afyon and the Isparta Angle. According to Koçyiğit (1984), the extensional tectonics commenced during the Miocene–Late Pleistocene; this period is interpreted as the beginning of intra-plate rifting. Yılmaz (1989) noted that the compressional regime in western Anatolia was replaced by an extensional regime and then by alkaline volcanism in Pliocene time. Francalanci *et al.* (2000) argued that the alkaline magmatism was associated with an extensional tectonic phase and occurred along N–S-trending tectonic line between Afyon to Isparta, named the Antalya fault zone. Along the fault zone, silica-saturated to strongly silica-undersaturated K-rich volcanic rocks and ultrapotassic rocks erupted (Savaşçın *et al.* 1995; Francalanci *et al.* 2000).

Field Description

The study area is located in the southernmost part of the Afyon volcanic province (Figure 2), ~6-km southwest of the town of Balçıkhisar. The stratigraphic framework of the study is represented by (1) melilite-leucitite lavas: they are the first products of the first volcanic activity; they intrude and cover the limestones of the Tauride belt; (2) leucitite blocks and a clast-rich volcaniclastic succession namely the Balçıkhisar volcaniclastic succession: they cover the first volcanic products and lamproitic rocks, which are one of the first products of a second magmatic phase; (3) lacustrine sedimentary rocks: they show gradational conformably boundary relationships with the underlying volcaniclastic succession and interfinger with the Tokluk volcano-sedimentary succession; (4) phonotephritic lava domes, dykes, and

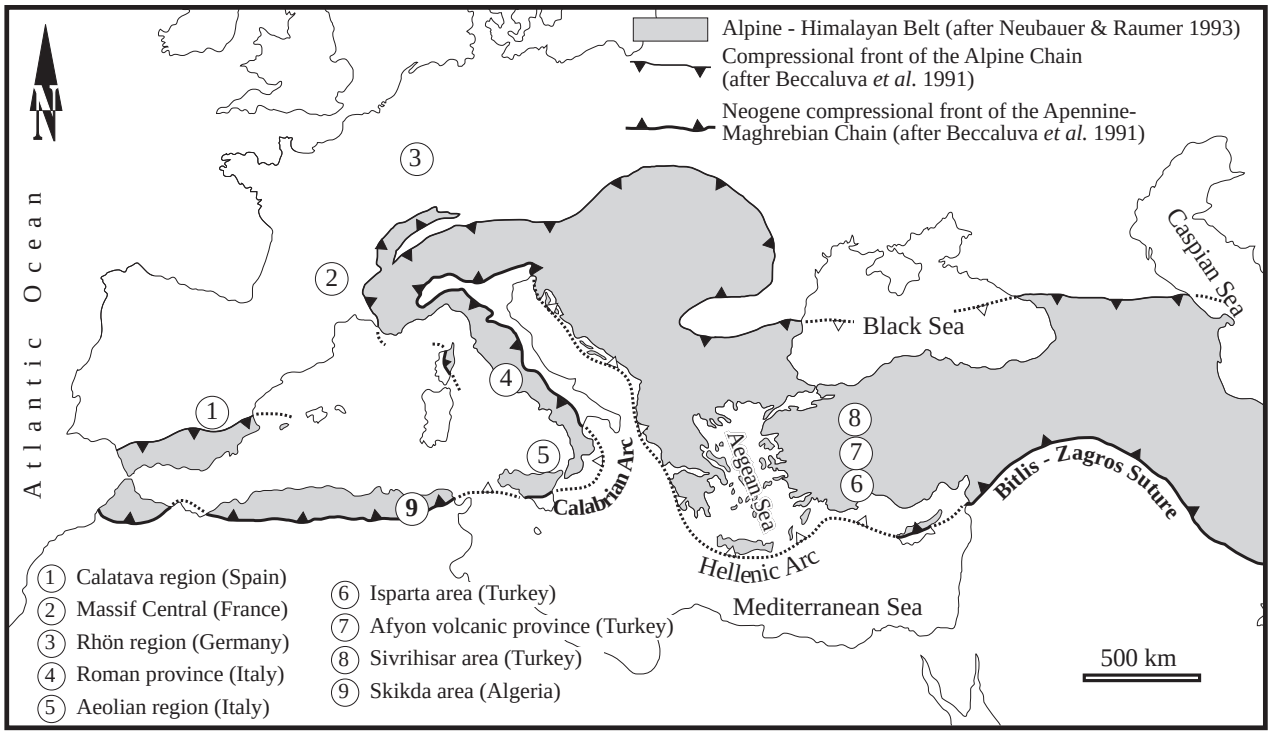

Figure 1. Structural sketch map of the Mediterranean region and the locations of potassium-rich volcanic rocks.

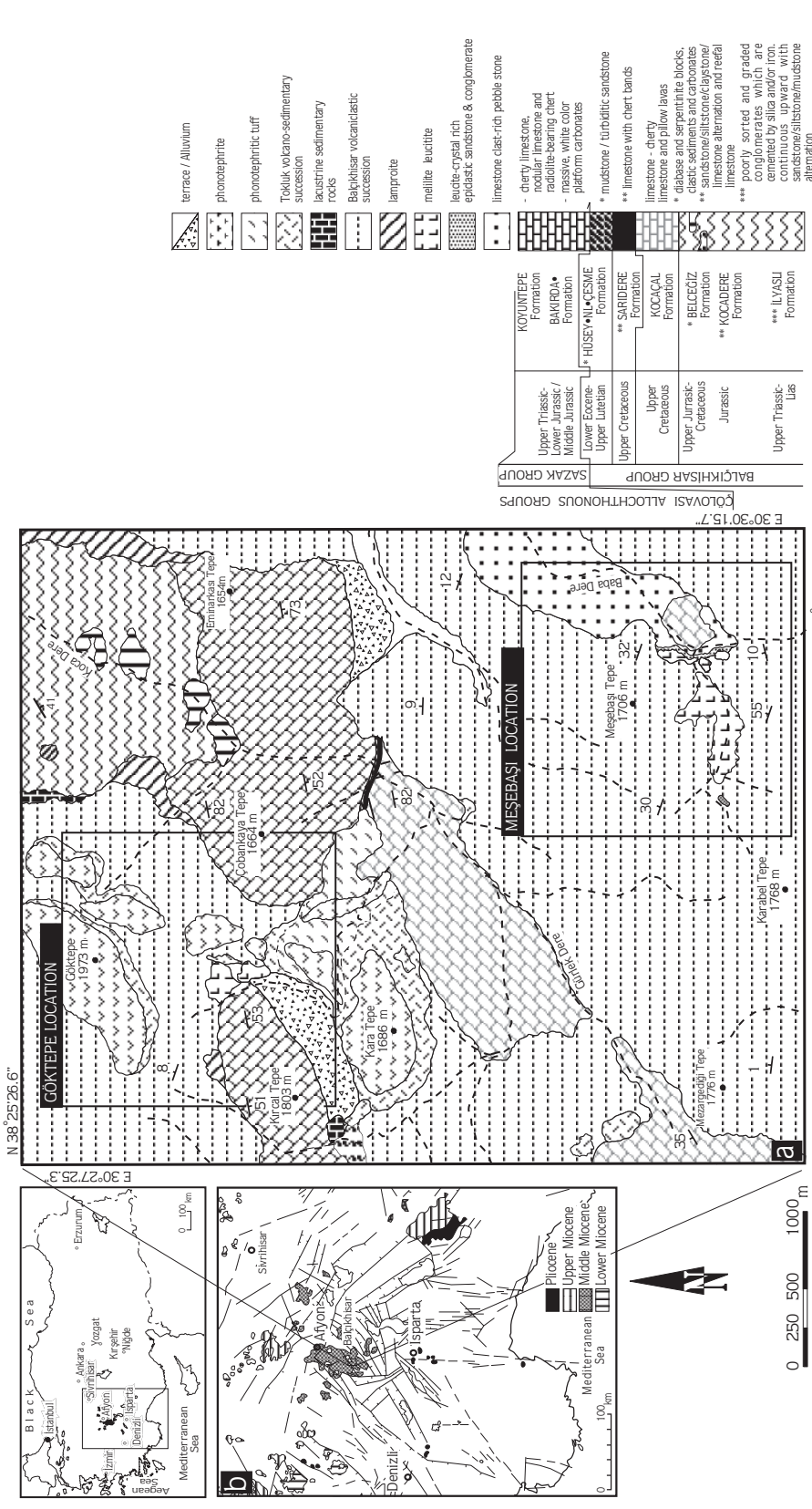

Figure 2. (a) Detailed geological map of the study area; (b) simplified map showing the major structural elements and Miocene volcanics of western and central Anatolia (modified from Bingöl 1989; Ercan 1979, 1986; Ercan *et al.* 1983; Innocenti *et al.* 1982; Kaya 1981, 1982; Koçyiğit 1984; Pasquare *et al.* 1988).

flows that characterise the third phase of volcanic activity in the area.

Melilite leucitites, originally emplaced as domes and spatially limited lava flows, crop out in two small creeks around Meşebaşı Tepe and Göktepe (Figure 2). Melilite-leucitite lavas at both locations are typically dark to light grey and have massive texture; euhedral and/or partially rounded leucite phenocrysts with a diameter ranging from 5 mm to 4 cm are characteristic (Figure 3).

Figure 3. Grey-dark grey massive leucitite lavas and euhedral leucite phenocrysts (white colour) in the melilite-leucitite lavas. The hammer is 33-cm long.

At the Meşebaşı location, the melilite leucitites are well exposed. The Balçıkhisar volcaniclastic deposits overlie a leucitite dome and related lava flows (Figure 4a, b). An unconformity between pyroclastic sequence and the melilite leucitites can be recognised from its light grey weathering surfaces. The thickness of the weathering zone is about 50 cm. The components of the weathering zone, which cause the development of the palaeosol, include fractured individual leucite crystals and melilite-leucitite clasts. The grains of the palaeosol are cemented by a carbonate matrix.

The melilite-leucitite lavas are underlain by euhedral leucite phenocryst-bearing epiclastic sandstone and conglomerate (Figure 4a, b). The sequence is composed of sand-sized crystal fragments of leucite, clinopyroxene, phlogopite and melilite-leucitite lithic clasts. Crystal fragments constitute more than 50 modal percent.

The sizes of euhedral leucite phenocrysts reach 4 cm (Figure 4c). The other components of the sequence consist of limestone, quartzite, and volcanic-rock fragments. The uppermost part of the sequence is rich in fine leucite crystals and crystal fragments. Throughout the sequence, a calcite matrix is common.

Petrography and Mineralogy of Melilite Leucitite

The melilite-leucitite lavas show typically hypocrystalline texture that is characterised by the presence of large euhedral leucite and euhedral/subhedral clinopyroxene phenocrysts (Figure 5). Melilite leucitites at both locations are composed of leucite, nepheline, melilite, diopside, melanite, calcite, apatite, and opaque minerals. Microphenocrysts are mainly leucite, nepheline, melilite, pyroxene, and rarely melanite, Ba-feldspar, and apatite. The rest of the matrix consists completely of leucite, melanite, apatite, clinopyroxene, and opaque microcrysts. The < 0.1 mm equant leucite crystals that comprise the majority of the groundmass show morphologies consistent with dodecahedral forms. The nepheline and leucite crystals as observed in the thin section are mantled by secondary calcite.

Leucites

Leucite occurs as twinned, weakly anisotropic euhedral crystals free of fluid inclusions; however, acicular apatite inclusions are common. Although coarsely crystalline, no chemical or optical zoning has been detected in the leucites. Representative analyses of these leucites are given in Table 1. The compositional range is narrow and very close to ideal leucite stoichiometry. These leucites have high Fe and very low Na and Ca contents relative to the analyses of leucite tabulated by Deer *et al.* (1993). Notably, significant Ba (up to 0.5 wt%) is present. The recalculated analyses show that the compositional range of the leucites is narrow and very close to ideal leucite in the SiO_2–$NaAlSiO_4$–$KAlSiO_4$ ternary diagram (Figure 6).

Ba-Feldspar

Barium feldspars, which have only been observed in the Meşebaşı melilite leucitite, are colourless anhedral crystals that are usually associated with leucite (Figure 7).

Symplectite intergrowth textures characterised the barium feldspars. Leucite crystals are probably replaced by Ba-feldspar. The colourless minerals contain up to 23 wt% BaO (Table 1). The sums of the microprobe analyses are close to 100 wt%, indicating that this is not hydrated.

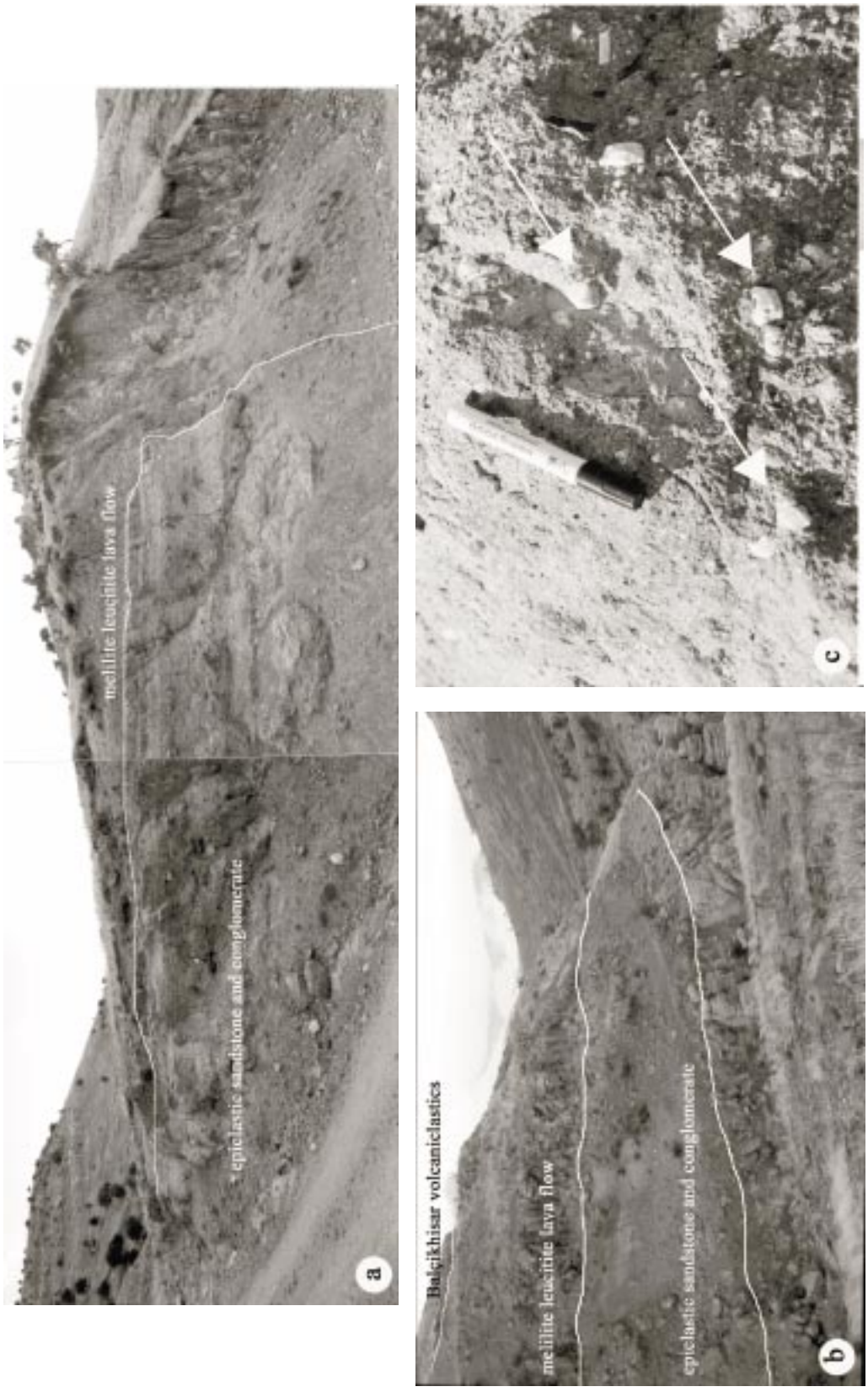

Figure 4. (a) Melilite-leucitite lavas overlie euhedral leucite-bearing epiclastic sandstone and conglomerate; (b) melilite-leucitite lava flows; (c) euhedral leucite phenocrysts in epiclastic sandstone and conglomerate. Pen is 14-cm long.

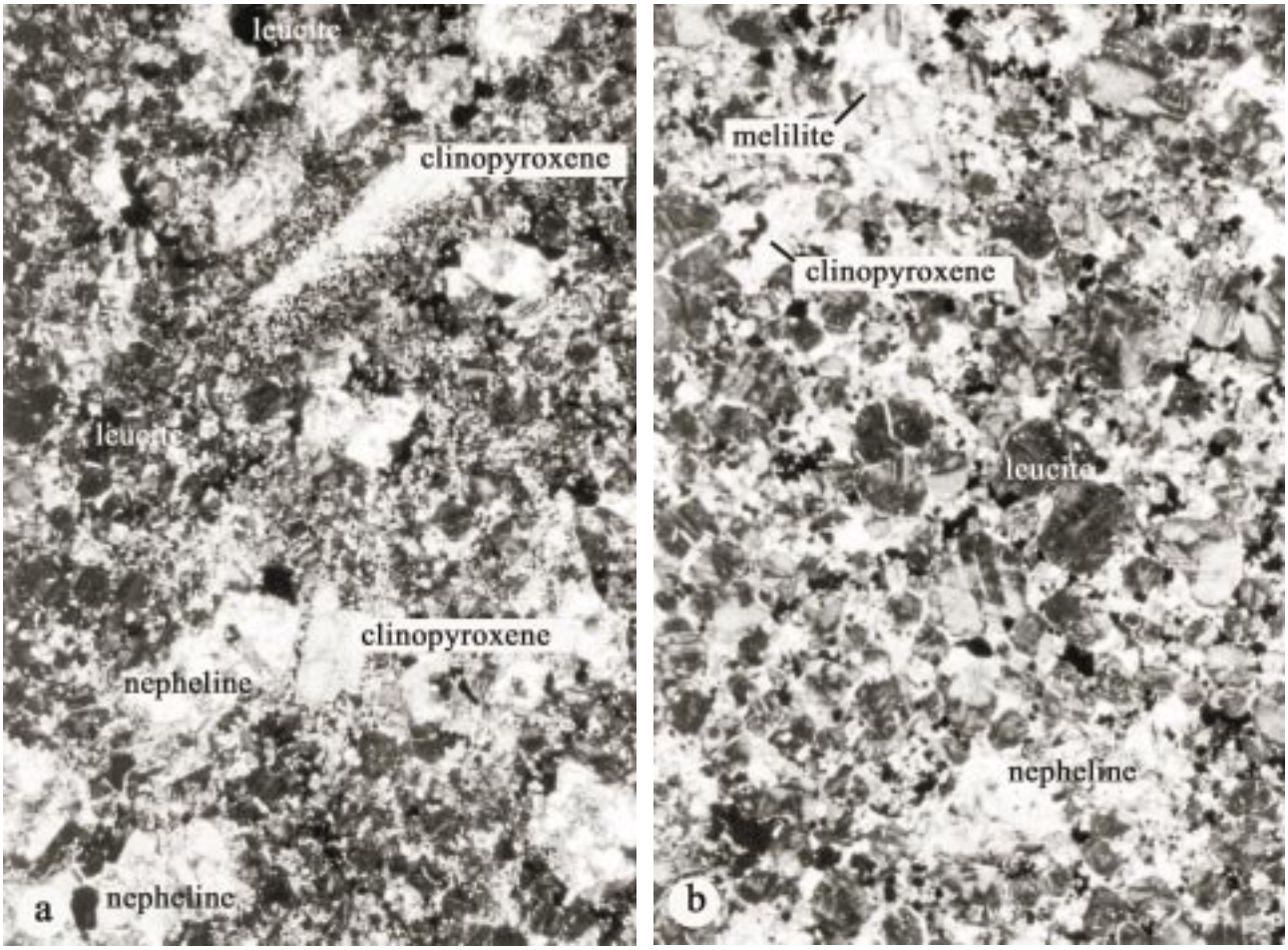

Figure 5. Photomicrograph of melilite leucitites hypocrystalline texture, comprising mainly leucite phenocrysts and scarce clinopyroxene phenocrysts (diopside in composition). The long side of the photographs are 4 mm in length, crossed-nicols.

The Ba-feldspar analyses are recalculated by using feldspar end-members, and the results were plotted onto Or-Ab-An ternary diagrams. All analyses plot in the orthoclase-sanidine field (Figure 8a).

Barium feldspar that coexists with leucite crystal was analysed. The microprobe traverses from barium feldspar to leucite show that K_2O and SiO_2 contents significantly increase and BaO significantly decrease in the leucite. However, the Al_2O_3 contents of the leucite are only slightly higher than those of the Ba-feldspar (Table 1; Figure 8b).

Nepheline

Nepheline is recognised by its square to hexagonal crystals. In these rocks, the nepheline crystals are typically mantled by calcite. Some of nepheline crystals have skeletal-like structures in the calcite matrix (Figure 5). Nepheline crystals in the Meşebaşı leucitite have compositions close to ideal nepheline (Table 1). In the SiO_2 (Q)–$NaAlSiO_4$ (Ne)–$KAlSiO_4$ (Ks) diagram, our nepheline analyses are similar to those of Deer *et al.* (1993) (Figure 6).

Clinopyroxenes

Oscillatory- and sector-zoned clinopyroxene phenocrysts are elongate prismatic, subhedral and/or anhedral crystals, with pleochroism from pale green to pale brownish-green in the melilite-leucitite lavas. Dark green diopsidic microcrysts have been classified into two subgroups; as groundmass (dark green, needle- and lath-

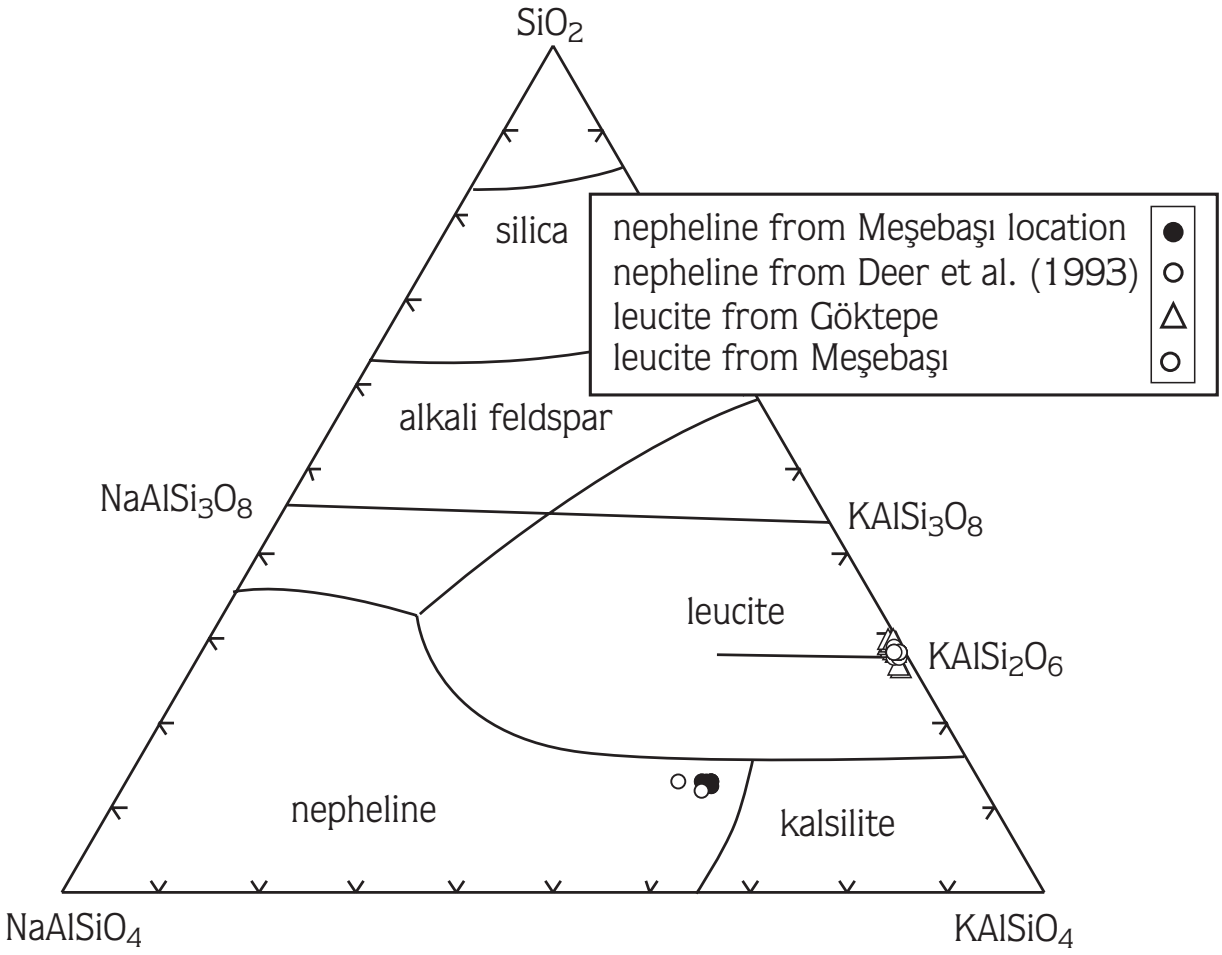

Figure 6. Recalculated analyses of leucite and nepheline are plotted in terms of SiO_2 (Q)-$NaAlSiO_4$ (Ne)-$KAlSiO_4$ (Ks). For comparison, some nepheline data are taken from Deer *et al.* 1993.

shaped tiny, crystals), and as microcrysts that are scattered in the groundmass. Representative analyses and calculated full-range compositions of the clinopyroxenes are presented in Table 2. Ferric iron contents were calculated by assuming that the pyroxenes are stoichiometric, with the sum of the cations equal to four on the basis of six oxygens.

Clinopyroxene phenocrysts are scarce in the melilite leucitite, and the analysed minerals generally plot on the Di-Hd join. As seen in Figure 9 (Marimoto 1989), the clinopyroxene phenocrysts in the Meşebaşı leucitite are diopsidic, and microcrysts are salitic in composition. In the Göktepe leucitite, the analysed microphenocrysts have diopside-salite/salite compositions.

Melilites

Melilites are the main mineralogical component of the Meşebaşı melilite-leucitite and are distinguished by their peg structure patterns and clearly identified by their orange yellow–pale blue interference colours and honey yellow–golden yellow pleochroism (Figure 10). The microcrystic melilites are the main components of the matrix.

The analysed melilite compositions are rather restricted, but one strontium-rich (up to 1.38 wt%). In terms of end-members, variations in composition can be represented by soda-melilite 27–31, gehlenite 25–38 and akermanite 31–46 as shown in Table 3 and Figure 11. All are relatively gehlenite-akermanite rich, soda-melilite proportions are low (Figure 11a)

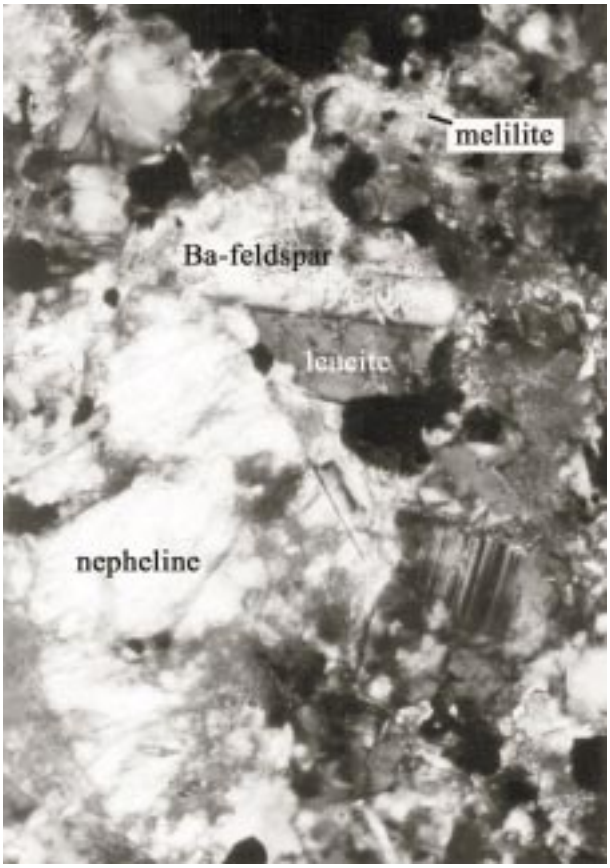

Figure 7. Barium feldspar, distinguished in thin sections by its symplectite-like intergrowth textures between leucite and barium feldspar. The long side of the photograph is 0.6 mm in length, crossed-nicols.

The compositions of the melilites are close to those reported by Sahama & Meyer (1958), Velde & Yoder (1977), and Toscani *et al.* (1990) from the Nyirogongo volcano and by Dunworth & Wilson (1998) from SW Germany (Figure 11b).

At the Meşebaşı location, the clinopyroxene phenocrysts are anhedral and completely or partially transformed to melilite. Good examples are presented in Figure 12. The upper left photograph (Figure 12a) shows a partially rounded a large diopside. The upper right photograph (Figure 12b) shows a clinopyroxene that is partially transformed to melilite. The lower left photograph (Figure 12c) shows clinopyroxene relicts that are enclosed in an aggregate of melilite. The uniform optical orientations of the clinopyroxene are preserved. In the last picture (Figure 12d) clinopyroxene has been completely transformed to melilite. Sahama (1968) suggested that decreasing temperature, clinopyroxene crystals react with the melt producing a margin of melilite. This transformation is explained as melilitisation of pyroxene by Borodin & Pavlenko (1974) and is a product of a metasomatic process in the formation of alkaline rocks. The clinopyroxenes are diopsidic. The melilite derived from clinopyroxene has the same composition as single melilite microphenocrysts.

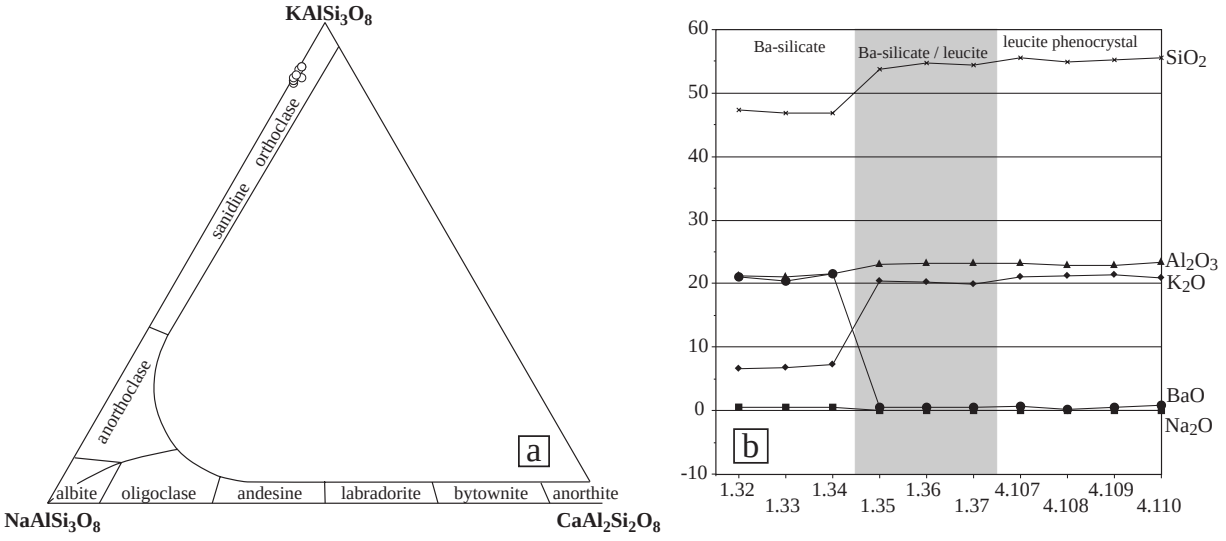

Figure 8. (a) Compositions of Ba-feldspar minerals on the Or–Ab–An ternary diagram; (b) compositional change from the Ba-feldspar mineral that coexists with leucite.

Table 1. Representative microprobe analyses of leucite, nepheline, Ba-feldspar crystals and a microprobe traverse from Ba-feldspar to leucite crystals.

	LEUCITITE											Ba-FELDSPAR								
Sample No	62	63	64	66	4.108	4.109	5.114	5.115	6.125	6.126	6.127	1.32	1.33	1.34	2.62	2.63	2.64	3.98	3.99	3.100
SiO_2	54.40	55.00	55.75	56.00	54.88	55.25	55.00	55.66	55.76	55.95	55.55	47.37	46.82	46.78	47.81	46.63	47.87	47.20	47.98	46.62
TiO_2	0.00	0.01	0.00	0.00	0.06	0.08	0.03	0.06	0.11	0.10	0.01	0.04	0.11	0.05	0.09	0.00	0.04	0.00	0.10	0.06
Al_2O_3	22.29	22.21	22.41	22.44	22.83	22.79	23.07	22.86	23.20	23.02	22.93	21.29	21.02	21.48	21.43	21.35	21.34	21.51	21.52	20.07
FeO	0.26	0.28	0.25	0.24	0.34	0.52	0.27	0.58	0.55	0.46	0.64	1.74	1.65	1.46	2.03	1.82	1.68	1.92	1.61	1.46
MgO	0.00	0.00	0.00	0.00	0.00	0.02	0.00	0.00	0.00	0.01	0.00	0.04	0.04	0.06	0.07	0.06	0.04	0.04	0.04	0.14
CaO	-	-	-	-	-	-	-	-	-	-	-	0.02	0.01	0.01	0.00	0.00	0.09	0.00	0.02	2.05
BaO	0.00	0.00	0.00	0.00	0.12	0.51	0.08	0.16	0.16	0.55	0.00	21.07	20.40	21.49	21.05	22.11	21.22	22.01	22.05	17.93
Na_2O	0.04	0.05	0.12	0.00	0.03	0.02	0.00	0.03	0.00	0.01	0.01	0.59	0.58	0.50	0.53	0.57	0.55	0.55	0.49	0.49
K_2O	21.77	22.25	21.84	21.76	21.16	21.35	21.51	21.30	21.00	20.62	20.78	6.58	6.74	7.25	7.13	6.64	7.23	7.02	7.38	7.67
Total	98.8	99.8	100.4	100.5	99.5	100.6	100.0	100.7	100.9	100.8	99.9	98.81	97.50	99.14	100.22	99.30	100.14	100.34	101.28	96.57
Σcation=4 on the basis of 6 oxygens												cations per 32 oxygens								
Si	2.00	2.00	2.02	2.03	2.01	2.01	2.00	2.02	2.02	2.03	2.03	2.57	2.56	2.54	2.53	2.52	2.54	2.50	2.51	2.53
Ti	0.00	0.00	0.00	0.00	0.00	0.00	0.00	0.00	0.00	0.00	0.00	0.00	0.00	0.00	0.00	0.00	0.00	0.00	0.00	0.00
Al	0.97	0.95	0.96	0.96	0.99	0.98	0.99	0.98	0.99	0.99	0.99	1.36	1.36	1.38	1.34	1.36	1.34	1.34	1.33	1.28
Fe^{+2}	0.01	0.01	0.01	0.01	0.01	0.02	0.01	0.02	0.02	0.01	0.02	0.08	0.08	0.07	0.09	0.08	0.08	0.09	0.07	0.07
Mg	0.00	0.00	0.00	0.00	0.00	0.00	0.00	0.00	0.00	0.00	0.00	0.00	0.00	0.01	0.01	0.00	0.00	0.00	0.00	0.01
Ca	-	-	-	-	-	-	-	-	-	-	-	0.00	0.00	0.00	0.00	0.00	0.01	0.00	0.00	0.12
Ba	0.00	0.00	0.00	0.00	0.00	0.01	0.00	0.00	0.00	0.01	0.00	0.45	0.44	0.46	0.44	0.47	0.44	0.46	0.45	0.38
Na	0.00	0.00	0.01	0.00	0.00	0.00	0.00	0.00	0.00	0.00	0.00	0.06	0.06	0.05	0.06	0.06	0.06	0.06	0.05	0.05
K	1.02	1.03	1.01	1.01	0.99	0.99	1.00	0.98	0.97	0.96	0.97	0.46	0.47	0.50	0.48	0.46	0.49	0.47	0.49	0.53

	NEPHELINE											Ba-FELDSPAR						LEUCITE		
Sample No	1.17	1.18	2.24	2.25	3.5	4.59	4.6	5.72	5.73	9.118	9.119	1.32	1.33	1.34	1.35	1.36	1.37	4.107	4.108	4.109	4.110
SiO_2	42.41	43.20	41.87	42.09	41.93	42.23	41.79	42.48	43.12	42.68	43.07	47.37	46.82	46.78	53.82	54.68	54.47	55.48	54.88	55.25	55.58
TiO_2	0.01	0.05	0.04	0.02	0.07	0.03	0.00	0.04	0.00	0.06	0.06	0.04	0.11	0.05	0.09	0.06	0.11	0.06	0.06	0.08	0.05
Al_2O_3	32.03	32.40	31.96	31.92	32.23	32.67	32.33	32.49	32.20	31.76	31.43	21.29	21.02	21.48	23.01	23.12	23.20	23.16	22.83	22.79	23.33
FeO*	2.10	2.51	3.11	2.88	2.75	2.51	2.61	2.21	2.10	2.51	2.35	1.74	1.65	1.46	0.33	0.55	0.63	0.33	0.34	0.52	0.66
MgO	0.09	0.09	0.07	0.09	0.08	0.04	0.07	0.13	0.05	0.06	0.08	0.04	0.04	0.06	0.02	0.00	0.01	0.01	0.00	0.02	0.00
CaO	0.05	0.03	0.00	0.02	0.02	0.03	0.08	0.02	0.02	0.08	0.11	0.02	0.01	0.01	0.00	0.00	0.00	0.00	0.00	0.00	0.03
BaO	-	-	-	-	-	-	-	-	-	-	-	21.07	20.40	21.49	0.47	0.47	0.51	0.74	0.12	0.51	0.82
Na_2O	15.23	15.27	15.18	15.02	15.58	15.21	15.38	15.13	15.08	15.53	15.41	0.59	0.58	0.50	0.02	0.01	0.01	0.02	0.03	0.02	0.05
K_2O	7.01	6.98	7.54	7.56	7.11	7.37	7.11	7.13	6.78	7.37	7.03	6.58	6.74	7.25	20.34	20.27	19.91	21.11	21.16	21.35	20.87
Total	99.00	100.65	99.78	99.67	99.91	100.23	99.53	99.90	99.47	100.16	99.71	98.81	97.50	99.14	98.27	99.30	98.86	101.0	99.5	100.6	101.5
cations per 32 oxygens																					
Si	2.11	2.12	2.07	2.09	2.07	2.08	2.07	2.10	2.14	2.10	2.13	2.57	2.56	2.54	1.98	1.98	1.98	2.01	2.01	2.01	2.01
Ti	0.00	0.00	0.00	0.00	0.00	0.00	0.00	0.00	0.00	0.00	0.00	0.00	0.00	0.00	0.00	0.00	0.00	0.00	0.00	0.00	0.00
Al	1.88	1.87	1.86	1.86	1.87	1.89	1.89	1.89	1.88	1.84	1.83	1.36	1.36	1.38	1.00	0.99	1.00	0.99	0.99	0.98	0.99
Fe	0.09	0.10	0.13	0.12	0.11	0.10	0.11	0.09	0.09	0.10	0.10	0.08	0.08	0.07	0.01	0.02	0.02	0.01	0.01	0.02	0.02
Mg	0.01	0.01	0.01	0.01	0.01	0.00	0.01	0.01	0.00	0.00	0.01	0.00	0.00	0.01	0.00	0.00	0.00	0.00	0.00	0.00	0.00
Ca	0.00	0.00	0.00	0.00	0.00	0.00	0.00	0.00	0.00	0.00	0.01	0.00	0.00	0.00	0.00	0.00	0.00	0.00	0.00	0.00	0.00
Ba	-	-	-	-	-	-	-	-	-	-	-	0.45	0.44	0.46	0.01	0.01	0.01	0.01	0.00	0.01	0.01
Na	1.47	1.45	1.46	1.44	1.49	1.45	1.48	1.45	1.45	1.48	1.48	0.06	0.06	0.05	0.00	0.00	0.00	0.00	0.00	0.00	0.00
K	0.44	0.44	0.48	0.48	0.45	0.46	0.45	0.45	0.43	0.46	0.44	0.46	0.47	0.50	0.95	0.94	0.92	0.98	0.99	0.99	0.96

Table 2. Representative microprobe analyses of clinopyroxene phenocrysts and microcrysts of the melilite leucitites.

	c	-	r	c	r	m	m	m	m	m	c	r	m	c
Sample No	27	3.26	3.28	3.40	3.39	122	123	19/a-1	19/a-2	19/a-3	19/a-4	19/a-5	19/a-6	19/a-7
SiO_2	51.71	54.05	51.35	52.41	52.49	51.33	49.56	50.67	50.01	50.33	51.24	51.21	52.54	52.66
ZrO_2	0.03	0.02	0.05	0.04	0.01	0.00	0.10	0.00	0.00	0.00	0.00	0.00	0.00	0.01
TiO_2	0.56	0.34	0.52	0.49	0.41	0.92	1.40	1.77	1.10	1.08	0.85	0.87	0.63	0.59
Al_2O_3	2.32	0.99	2.44	2.06	1.20	0.99	1.63	3.33	4.09	4.08	3.50	3.33	2.29	2.11
Cr_2O_3	0.00	0.00	0.00	0.00	0.00	0.00	0.00	0.00	0.05	0.16	0.08	0.07	0.02	0.01
FeO*	5.08	2.99	5.39	4.45	4.00	12.98	12.09	10.82	6.78	6.81	6.48	6.30	6.20	5.95
MnO	0.07	0.04	0.00	0.18	0.07	0.42	0.40	0.31	0.09	0.17	0.14	0.10	0.16	0.15
MgO	14.69	17.04	14.47	15.21	16.18	9.94	11.07	10.54	12.96	12.89	13.34	13.51	13.74	14.01
CaO	24.74	25.15	24.74	24.64	25.07	21.15	22.28	21.07	23.95	23.80	23.99	23.93	24.14	23.96
SrO	0.05	0.00	0.01	0.08	0.09	0.08	0.03	0.00	0.00	0.00	0.00	0.00	0.00	0.00
Na_2O	0.20	0.15	0.23	0.19	0.27	1.71	1.25	1.86	0.38	0.34	0.32	0.31	0.29	0.34
K_2O	0.00	0.02	0.00	0.00	0.00	0.01	0.02	0.15	0.01	0.02	0.01	0.00	0.04	0.03
Total	99.44	100.83	99.18	99.95	99.88	99.52	99.83	100.52	99.42	99.67	99.95	99.63	100.50	99.82
Calculated values assuming Scation =4 on the basis of 6 Oxygen atoms														
Si	1.92	1.95	1.91	1.93	1.92	1.95	1.87	1.89	1.87	1.88	1.90	1.90	1.94	1.95
Al	0.10	0.04	0.11	0.09	0.05	0.04	0.07	0.15	0.18	0.18	0.15	0.15	0.10	0.09
Ti	0.02	0.01	0.01	0.01	0.01	0.03	0.04	0.05	0.03	0.03	0.02	0.02	0.02	0.02
Cr	0.00	0.00	0.00	0.00	0.00	0.00	0.00	0.00	0.00	0.00	0.00	0.00	0.00	0.00
Fe^{2+**}	0.10	0.05	0.10	0.10	0.03	0.28	0.19	0.22	0.16	0.18	0.18	0.18	0.19	0.19
Fe^{3+**}	0.05	0.04	0.06	0.04	0.09	0.13	0.19	0.12	0.05	0.03	0.02	0.02	0.00	0.00
Mn	0.00	0.00	0.00	0.01	0.00	0.01	0.01	0.01	0.00	0.01	0.00	0.00	0.01	0.00
Mg	0.81	0.92	0.80	0.83	0.88	0.56	0.62	0.59	0.72	0.72	0.74	0.75	0.76	0.77
Ca	0.98	0.97	0.98	0.97	0.98	0.86	0.90	0.84	0.96	0.95	0.95	0.95	0.96	0.95
Na	0.01	0.01	0.02	0.01	0.02	0.13	0.09	0.13	0.03	0.02	0.02	0.02	0.02	0.02
K	0.00	0.00	0.00	0.00	0.00	0.00	0.00	0.01	0.00	0.00	0.00	0.00	0.00	0.00
Wo	50.29	49.09	50.41	49.87	49.38	46.55	46.96	47.43	50.58	50.44	50.27	50.14	50.06	49.69
En	41.54	46.28	41.02	42.82	44.37	30.42	32.48	33.02	38.09	38.01	38.90	39.39	39.65	40.43
Fs	8.16	4.63	8.57	7.31	6.25	23.02	20.56	19.56	11.33	11.55	10.83	10.47	10.30	9.88

c-1 .... m-10: Microprobe traverses for each phenocryst, from the central parts to the margins of the crystals
FeO^*: Total iron as FeO, in the atomic ratios
Fe^{2+**} & Fe^{3+**} Fe^{2+} and Fe^{3+} have been recalculated after Marimoto (1989)
c: core
r: rim
m: groundmass microcrysts

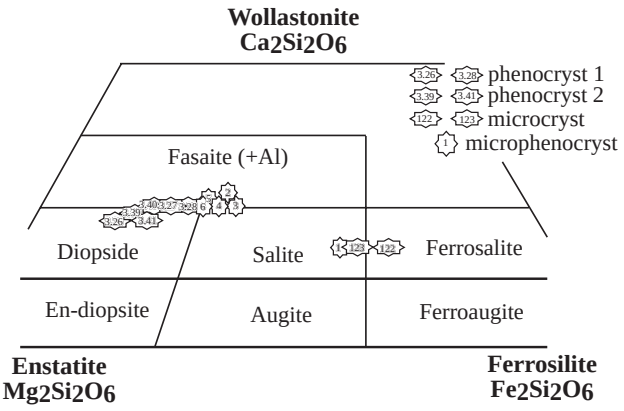

Figure 9. The composition of the clinopyroxene phenocrysts and microphenocrysts in the melilite-leucitite lavas.

Melanite

Melanite crystals are the main components of the melilite leucitites (Figure 13a). The garnet data are presented in Table 4. A notable feature is that the melanites are Ca- and Ti-rich garnet (up to 33 wt% CaO and up to 17.88 wt% TiO_2). Aluminium in the melanites is typically low (0.3–1.7 wt% Al_2O_3). While SiO_2, FeO, Na_2O, and K_2O decrease from the core to the margins of the crystals, TiO_2 and CaO increase.

Apatite

Apatite crystals are observed as subhedral/anhedral crystals and as acicular, euhedral crystals.

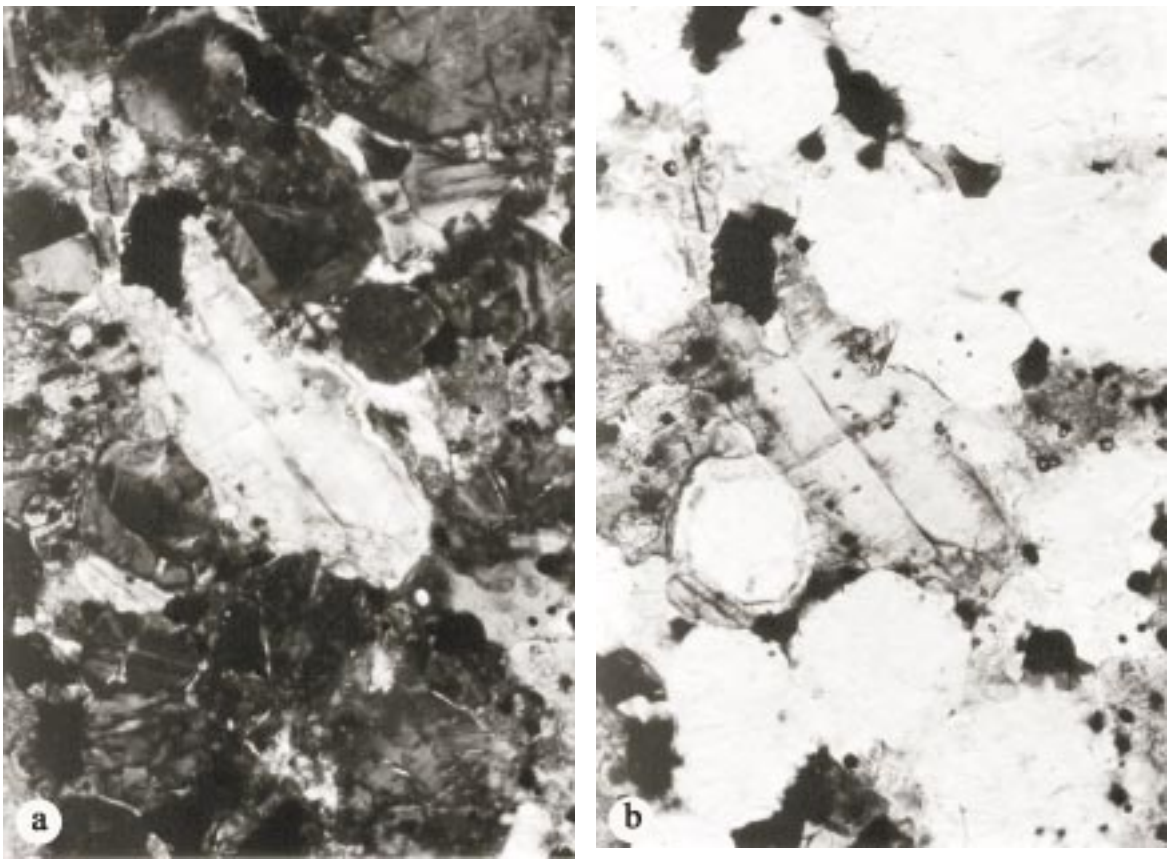

Figure 10. Melilite microphenocrysts and the peg structure pattern of the melilite crystals (sample from the Meşebaşı location). The long sides of the photographs are 1.1 mm in length, crossed-nicols and plane-polarised light.

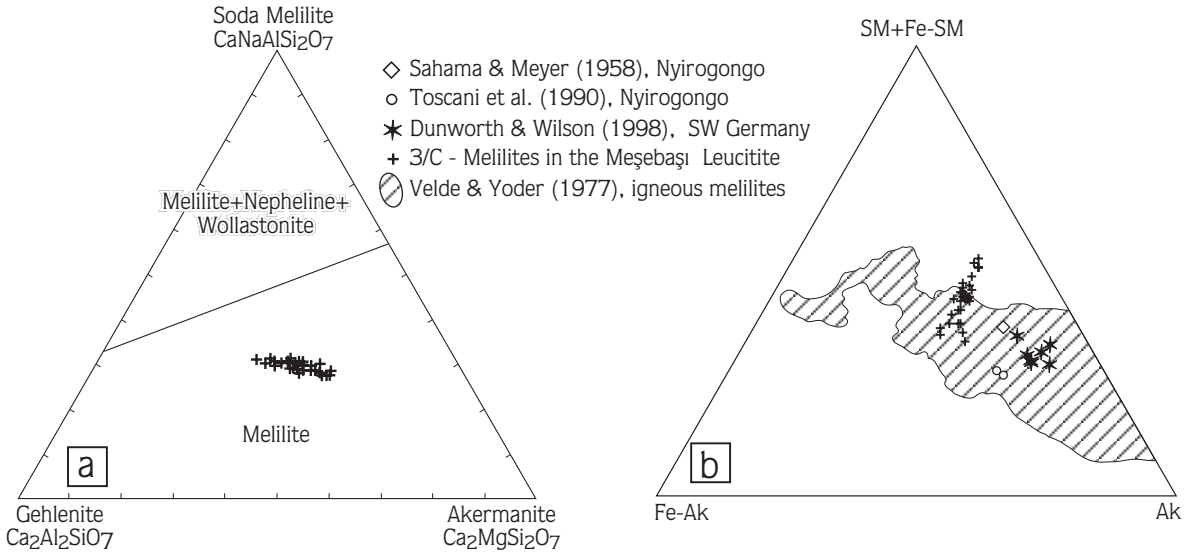

Figure 11. (a) Meşebaşı melilite compositions in terms of end-members; (b) comparison of the melilites from the Meşebaşı leucitite with volcanic melilites in the system soda-melilite -ferro-akermanite–akermanite.

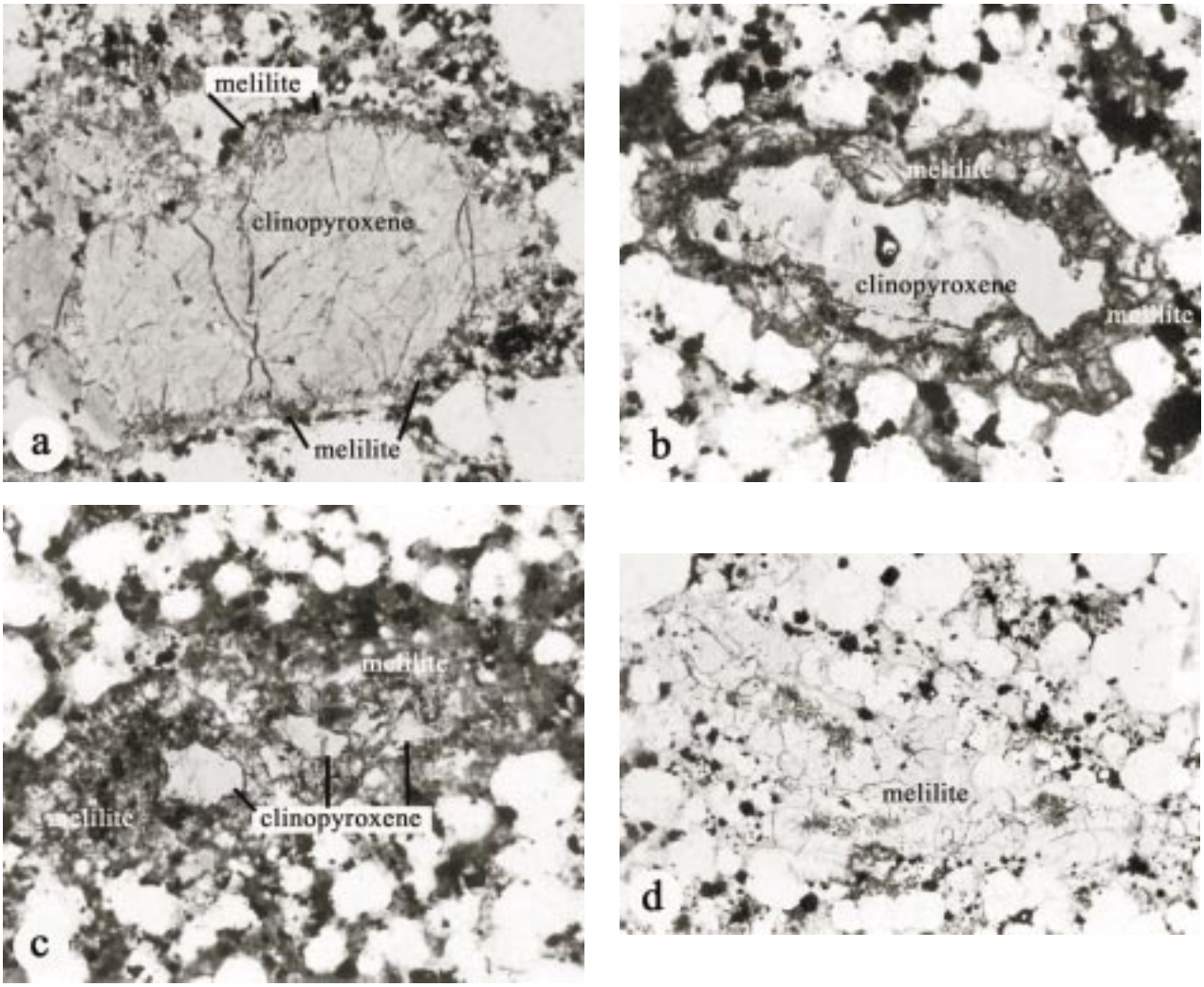

Figure 12. Melilite phenocrysts transformed from clinopyroxene. (a) Partly rounded large diopsidic clinopyroxene; (b) clinopyroxene, partly transformed to melilite; (c) clinopyroxene remnants enclosed in aggregates of melilite; (d) clinopyroxene is completely transformed to melilite aggregates. The long sides of the photographs are 1.5 mm in length, and crossed-nicols.

Subhedral/anhedral crystals, distinguished by their high relief and numerous highly refringent inclusions, are located in the groundmass (Figure 13b). Generally, the acicular apatite crystals are found as inclusions in leucite crystals. Chemical analyses for major elements (Table 5) show that these apatites are relatively homogeneous in composition (P_2O_5 ranges from 39 to 41 wt%, and CaO from 54 to 56 wt%). All of the crystals are fluor-apatite, with F ranging from 2.50 to 3.86 wt%.

Geochemistry

The major- and trace-element compositions of ten representative melilite-leucititic lava samples, including lava flows and lava domes, were determined by X-ray fluorescence spectrometry (XRF) on an ARL 8420 instrument in the Geoscience Analytical Services laboratories of Keele University (England), calibrated against both international and internal standards. REE were determined by ICP/MS at XRAL Laboratories (a division of SGS Canada Inc.).

Table 3. Representative microprobe analyses of melilite microphenocrysts from the Meşebaşı leucitite.

Sample No	1.4	1.6	2.13	2.15	4.43	4.44	5.53	7.68	7.71	8.84	8.85	9.88	9.90	10.94	10.95
SiO_2	42.00	42.65	42.05	42.39	42.13	42.49	42.79	43.28	42.47	42.70	42.33	43.20	43.15	42.77	42.19
TiO_2	0.10	0.03	0.00	0.05	0.00	0.05	0.06	0.00	0.03	0.10	0.07	0.09	0.01	0.04	0.03
Al_2O_3	6.80	6.73	6.64	4.99	6.44	6.61	6.17	6.61	6.01	6.45	6.52	6.63	6.70	6.79	6.62
FeO	6.38	6.78	6.53	7.26	6.84	6.68	6.31	6.78	7.40	6.21	6.34	6.01	6.27	6.78	6.66
MnO	0.26	0.23	0.30	0.16	0.18	0.20	0.16	0.23	0.28	0.17	0.25	0.17	0.23	0.15	0.20
MgO	5.44	5.15	5.26	5.91	5.47	5.29	5.80	5.34	5.42	5.29	5.44	5.31	5.53	5.24	5.08
CaO	31.60	30.75	31.11	31.60	30.84	30.60	31.43	30.67	31.31	31.14	30.91	31.33	30.95	30.31	30.31
SrO	1.26	1.35	1.24	1.38	1.38	1.26	1.17	1.34	1.36	1.22	1.23	1.31	1.05	1.25	1.24
BaO	0.04	0.58	0.58	0.16	0.58	0.23	0.04	0.12	0.12	0.43	0.00	0.51	0.47	0.58	0.00
Na_2O	4.94	4.71	4.60	3.86	4.49	4.62	4.16	4.34	4.42	4.62	4.50	4.70	4.58	4.84	4.65
K_2O	0.08	0.19	0.12	0.12	0.09	0.09	0.09	0.15	0.15	0.11	0.13	0.10	0.11	0.16	0.09
Total	98.93	99.15	98.48	97.89	98.43	98.13	98.20	98.91	98.97	98.44	97.72	99.37	99.10	98.94	97.13
Si	3.89	3.97	3.94	4.01	3.95	3.99	4.01	4.04	3.96	3.99	3.98	4.00	4.01	3.98	3.99
Ti	0.01	0.00	0.00	0.00	0.00	0.00	0.00	0.00	0.00	0.01	0.01	0.01	0.00	0.00	0.00
Al	0.74	0.74	0.73	0.56	0.71	0.73	0.68	0.73	0.66	0.71	0.72	0.72	0.73	0.75	0.74
Fe^{3+}	0.36	0.19	0.23	0.13	0.21	0.14	0.06	0.01	0.23	0.14	0.15	0.12	0.09	0.18	0.13
Fe^{2+}	0.14	0.34	0.28	0.44	0.32	0.38	0.44	0.52	0.34	0.35	0.35	0.35	0.40	0.35	0.40
Mn	0.02	0.02	0.02	0.01	0.01	0.02	0.01	0.02	0.02	0.01	0.02	0.01	0.02	0.01	0.02
Mg	0.75	0.71	0.73	0.83	0.76	0.74	0.81	0.74	0.75	0.74	0.76	0.73	0.77	0.73	0.72
Ca	3.13	3.07	3.12	3.20	3.10	3.08	3.16	3.06	3.13	3.12	3.11	3.11	3.08	3.02	3.07
Sr	0.07	0.07	0.07	0.08	0.08	0.07	0.06	0.07	0.07	0.07	0.07	0.07	0.06	0.07	0.07
Ba	0.00	0.02	0.02	0.01	0.02	0.01	0.00	0.00	0.00	0.02	0.00	0.02	0.02	0.02	0.00
Na	0.89	0.85	0.84	0.71	0.82	0.84	0.76	0.79	0.80	0.84	0.82	0.84	0.82	0.87	0.85
K	0.01	0.02	0.01	0.01	0.01	0.01	0.01	0.02	0.02	0.01	0.02	0.01	0.01	0.02	0.01
SM-Fe.SM	55	47	48	35	46	43	37	36	44	44	43	43	41	46	44
Fe-AK	8	18	15	23	17	20	23	27	18	18	19	19	21	18	21
AK	37	36	37	42	38	37	41	37	37	38	38	38	38	36	36
SM	31	30	30	27	29	30	28	28	29	30	29	31	29	31	30
GEH	38	32	34	25	32	30	27	26	32	30	31	30	29	32	30
AK	31	37	36	48	39	40	46	46	40	39	40	39	41	37	39

Calculated values assuming Scation =10 on the basis of 14 Oxygen atoms

FeO*: Total iron as FeO, in the atomic ratios

Fe^{2+**} & Fe^{3+**}: Fe^{2+} and Fe^{3+} have been recalculated after Marimoto (1989)

Quantitative analyses of mineral compositions were obtained at the Universite Pierre et Marie Curie (Laboratoire de Petrologie-Mineralogique), Paris using MS-46 CAMECA electron microprobe and CAMEBAX automated electron microprobe. Natural and synthetic minerals were used as standards for clinopyroxenes, amphiboles, micas, melilites, leucites, feldspars, and apatites. Counting time was 30s; accelerating voltage was 15kV; beam current was 20–30nA; beam diameter was 5 µm.

Bulk rock major- and trace-element analyses and CIPW norms of the representative melilite-leucitite samples are presented in Table 6. The melilite-leucitite lavas are highly Ba, Zr and K-rich and strongly alkaline, and plot in the leucite field in the total alkali-silica classification of Le Bas *et al.* (1986) (Figure 14a, b).

The selected representative samples are plotted on the Ce/Zr versus Zr binary diagram of Floyd *et al.* (1996) for partial melting and fractional crystallisation processes for the melilite leucitite. The diagram uses possible crustal

Table 4. Representative microprobe analyses of Ti-rich melanite crystals from the Göktepe and Meşebaşı leucitites.

	inner-1	2	3	4	5	6	edge7	inner-1	2	edge-3
Sample No				19/A					3/C	
Analyse No	56	57	58	59	60	61	1.7	4.61	4.76	4.77
SiO_2	51.94	35.26	29.18	28.71	28.06	28.33	26.37	53.87	22.67	24.52
TiO_2	0.62	2.26	13.56	14.71	15.13	14.97	17.01	0.10	16.32	17.49
Al_2O_3	0.53	0.50	0.32	0.35	0.38	0.39	0.67	23.21	1.70	1.07
FeO*	15.46	27.66	22.47	21.89	22.07	21.56	19.98	0.61	18.53	19.04
MnO	0.58	0.27	0.37	0.42	0.36	0.39	0.35	0.06	0.18	0.26
MgO	8.76	0.24	0.60	0.66	0.69	0.75	0.96	0.00	0.92	1.14
CaO	19.55	33.13	31.46	31.92	31.48	31.31	31.61	0.05	30.69	31.22
Na_2O	2.61	0.08	0.44	0.43	0.51	0.44	0.36	0.00	0.04	0.16
K_2O	0.12	0.02	0.00	0.01	0.00	0.00	0.00	19.97	0.00	0.00
Total	100.23	99.48	98.40	99.13	98.71	98.15	97.47	98.86	95.50	96.62
Calculated values assuming Scation =8 on the basis of 12 Oxygen atoms										
Si	3.93	2.91	2.48	2.42	2.38	2.41	2.27	4.00	2.04	2.15
Ti	0.04	0.14	0.87	0.93	0.96	0.96	1.10	0.01	1.10	1.15
Al	0.05	0.05	0.03	0.03	0.04	0.04	0.07	2.03	0.18	0.11
Fe^{+3}	0.41	1.87	1.36	1.33	1.36	1.29	1.24	-0.15	1.17	1.18
Fe^{+2}	0.56	0.04	0.23	0.21	0.20	0.25	0.20	0.19	0.22	0.21
Mn	0.04	0.02	0.03	0.03	0.03	0.03	0.03	0.00	0.01	0.02
Mg	0.99	0.03	0.08	0.08	0.09	0.10	0.12	0.00	0.12	0.15
Ca	1.58	2.93	2.86	2.88	2.86	2.86	2.91	0.00	2.95	2.93
Na	0.38	0.01	0.07	0.07	0.08	0.07	0.06	0.00	0.01	0.03
K	0.01	0.00	0.00	0.00	0.00	0.00	0.00	1.89	0.00	0.00

FeO*: Total iron as FeO. in the atomic ratios

Fe^{2+**} & Fe^{3+**}: Fe^{2+} and Fe^{3+} have been recalculated after Marimoto (1989)

Table 5. Representative microprobe analyses of apatite crystals in melilite-leucitite.

Sample No	23	24	25	26	27	28	29	30	32	33	34
SiO_2	1.34	1.32	2.04	1.16	1.31	2.12	1.85	1.51	1.86	1.98	1.83
MnO	0.00	0.00	0.05	0.06	0.00	0.00	0.00	0.04	0.04	0.09	0.00
CaO	56.39	56.50	55.37	55.91	55.99	54.39	54.91	55.84	56.37	55.90	55.81
SrO	0.59	0.85	1.46	0.30	0.76	0.65	0.67	0.73	0.84	1.06	0.42
Na_2O	0.05	0.03	0.04	0.05	0.06	0.04	0.07	0.05	0.05	0.06	0.05
P_2O_5	40.93	41.09	38.37	40.40	40.24	37.46	39.32	40.07	39.60	39.36	39.16
La_2O_3	0.13	0.16	0.42	0.11	0.06	0.54	0.20	0.14	0.20	0.22	0.09
Ce_2O_3	0.14	0.25	0.73	0.06	0.21	0.76	0.66	0.16	0.27	0.35	0.37
Nd_2O_3	0.00	0.11	0.28	0.15	0.27	0.35	0.13	0.29	0.07	0.29	0.06
F	2.77	2.50	2.80	3.68	3.55	3.33	3.86	3.56	3.18	3.36	3.13
Cl	0.02	0.01	0.01	0.06	0.00	0.01	0.00	0.00	0.01	0.00	0.03
Total	102.36	102.81	101.57	101.95	102.44	99.64	101.67	102.40	102.53	102.66	101.05

Table 6. Major- (wt%), trace- (ppm) and rare-earth element compositions of selected samples of melilite leucitites with C.I.P.W. norms.

	MEŞEBAŞI LOCATION								GÖKTEPE LOCATION		
Sample No	1a	1c	1d	2g	3b	3c	3d	18	19a	19b	19c
SiO_2	46.16	45.60	46.89	46.14	45.64	46.05	46.04	48.92	45.62	44.02	45.28
TiO_2	1.04	1.00	1.06	1.04	1.01	0.98	1.02	1.44	1.27	1.22	1.25
Al_2O_3	17.96	17.52	18.05	17.74	17.44	17.57	17.55	16.80	16.45	15.80	16.13
Fe_2O_3T	6.52	6.36	6.59	6.50	6.44	6.40	6.46	8.38	7.06	6.87	7.11
MnO	0.12	0.11	0.12	0.12	0.11	0.12	0.12	0.17	0.13	0.13	0.14
MgO	1.61	1.69	2.37	1.83	2.14	1.79	1.87	1.99	2.88	3.57	2.57
CaO	9.76	9.61	7.48	8.07	9.07	9.91	8.84	6.41	9.36	9.17	10.59
Na_2O	2.00	1.65	2.27	1.98	1.29	1.96	2.04	2.60	1.83	2.44	3.00
K_2O	11.24	11.25	12.02	11.81	11.19	10.09	11.67	9.69	9.46	9.76	8.48
P_2O_5	0.28	0.26	0.27	0.27	0.31	0.30	0.31	0.28	0.50	0.48	0.49
LOI	2.56	3.47	2.41	2.48	3.47	4.62	2.27	1.88	3.98	4.28	3.14
Total	98.97	98.53	99.55	97.98	98.13	99.78	98.17	98.56	98.53	97.74	98.17
Cl	620	557	1048	1299	433	210	1038	827	241	1479	1403
S	386	233	239	294	196	109	519	61	162	233	148
Cr	24	35	27	24	29	25	23	49	25	28	33
Cu	83	82	77	84	90	77	86	131	109	100	121
Ga	22	24	24	22	22	23	24	26	24	25	27
Nb	41	41	44	44	41	40	42	52	47	45	47
Ni	10	8	11	9	9	9	11	13	16	17	21
Pb	99	94	77	97	97	85	103	86	121	121	122
Rb	433	486	656	670	505	373	506	513	480	498	518
Sr	3227	3702	2490	3234	4802	3010	3419	3031	2222	2811	3984
Th	54	50	58	52	55	61	51	54	72	61	61
V	140	142	142	130	122	114	124	214	168	165	172
Y	28	27	28	30	26	22	28	36	36	34	34
Zn	97	96	99	95	98	97	99	110	110	109	110
Zr	568	530	587	601	542	425	565	857	769	761	772
Ba	4951	4976	6055	5402	5064	4701	5177	6882	8745	6618	6510
La	77	71	80	67	71	74	64	97	116	93	103
Ce	122	111	119	114	128	120	101	155	184	185	163
Nd	43	36	40	40	42	40	34	40	57	53	51
or (KAS6)	29.10	28.12	15.37	22.55	22.31	36.26	24.32	55.40	28.36	69.89	39.89
an (CAS2)	7.50	8.01	3.84	5.12	9.85	10.46	4.68	6.22	9.94	-	6.21
lc(KAS4)	35.18	36.95	49.71	43.98	41.56	24.47	41.65	7.62	28.19	-	13.70
ne(NAS2)	10.19	8.55	11.52	10.21	6.72	10.15	10.48	13.53	9.63	-	15.72
ns(NS)	-	-	-	-	-	-	-	-	-	9.05	-
Di wo(CS)	5.42	5.75	7.83	6.39	7.27	6.09	6.31	6.88	9.85	0.35	8.79
Di en(MS)	4.48	4.78	6.56	5.15	6.09	5.06	5.24	5.65	8.28	0.29	7.35
Di fs(FS)	0.25	0.24	0.25	0.47	0.23	0.26	0.25	0.36	0.28	0.01	0.30
Hy en(MS)	-	-	-	-	-	-	-	-	-	10.53	-
Hy fs(FS)	-	-	-	-	-	-	-	-	-	0.29	-
Ol fo(M2S)	-	-	-	-	-	-	-	-	-	0.47	-
Ol fa(F2S)	-	-	-	-	-	-	-	-	-	0.01	-
Total	92.11	92.39	95.10	93.86	94.02	92.74	92.93	95.66	94.54	90.89	91.96

REE compositions of samples			
		19a Göktepe	1a Meşebaşı
Au	(ppb)	5	<5
Na	(ppm)	>10000	>10000
Ca	(%)	7.4	6.6
Sc	(ppm)	5.4	2.7
Cr	(ppm)	20	14
Fe	(%)	4.45	3.7
Co	(ppm)	16	12
Ni	(ppm)	<100	<100
Zn	(ppm)	100	60
As	(ppm)	8	5
Se	(ppm)	<3	<3
Br	(ppm)	4	4
Rb	(ppm)	470	350
Sr	(ppm)	2200	2600
Mo	(ppm)	<5	<5
Ag	(ppm)	<5	<5
Sb	(ppm)	1.2	2
Cs	(ppm)	12	15
Ba	(ppm)	7500	4300
La	(ppm)	138	96
Ce	(ppm)	243	169
Nd	(ppm)	93	68
Sm	(ppm)	15.4	10.8
Eu	(ppm)	3.7	2.7
Tb	(ppm)	1.3	0.8
Yb	(ppm)	2.4	1.6
Lu	(ppm)	0.33	0.26
Hf	(ppm)	15	11
Ta	(ppm)	2	2
W	(ppm)	3	3
Ir	(ppb)	<20	<20
Hg	(ppm)	<1	<1
Th	(ppm)	58	43
U	(ppm)	19.1	18
Ce/Yb	(ppm)	101.25	105.63
Ba/Rb	(ppm)	16	12
Rb/Cs	(ppm)	39	23
La/Yb	(ppm)	58	60
Rb/Sr	(ppm)	0.21	0.13

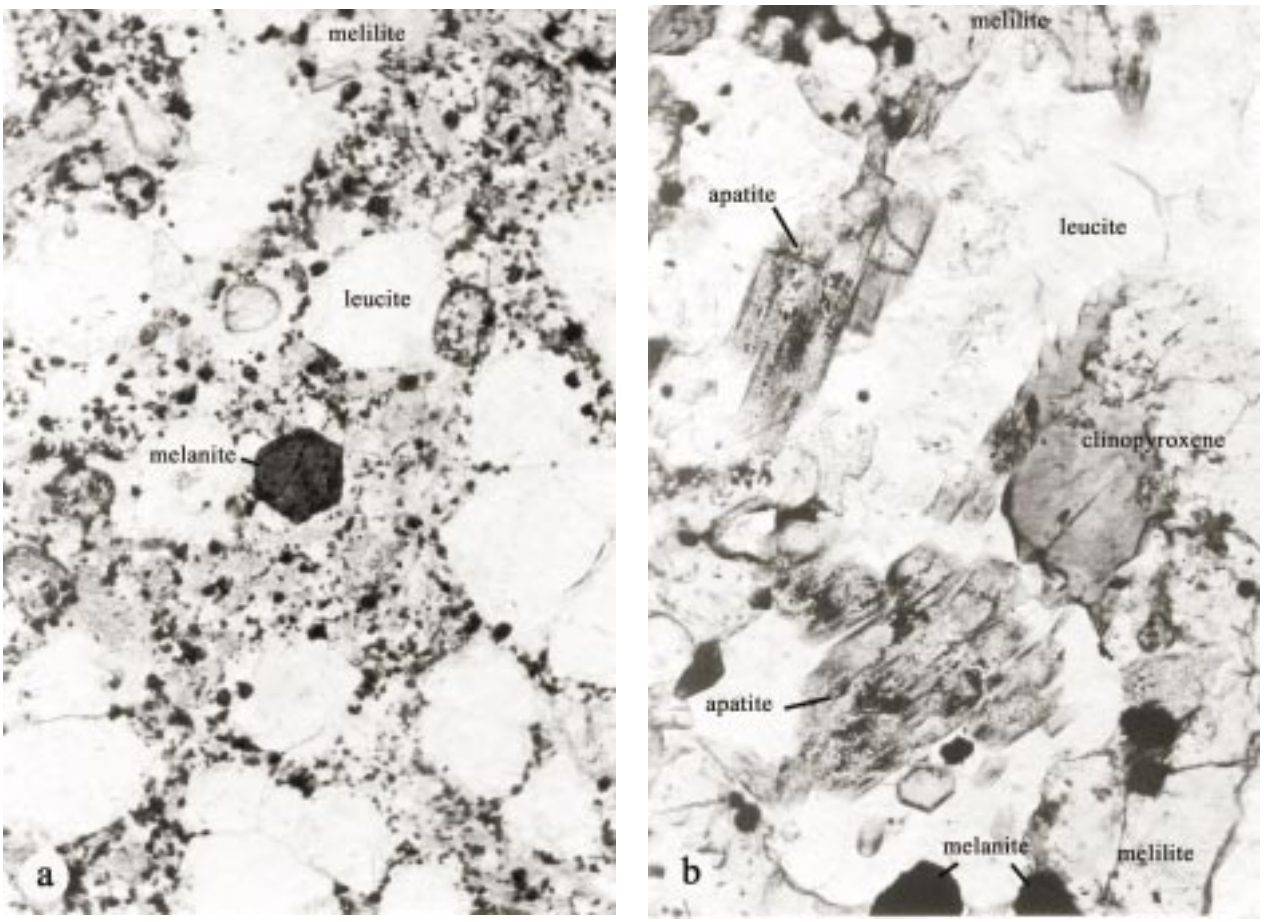

Figure 13. (a) Euhedral melanite microphenocrysts (micro-sized melanite crystals), distinguished by their dark brown colour in the groundmass; (b) apatite microphenocrysts are determined on the basis of their high relief and numerous high refringent inclusions. The long sides of the photographs are 0.7 mm in length, plane-polarised light.

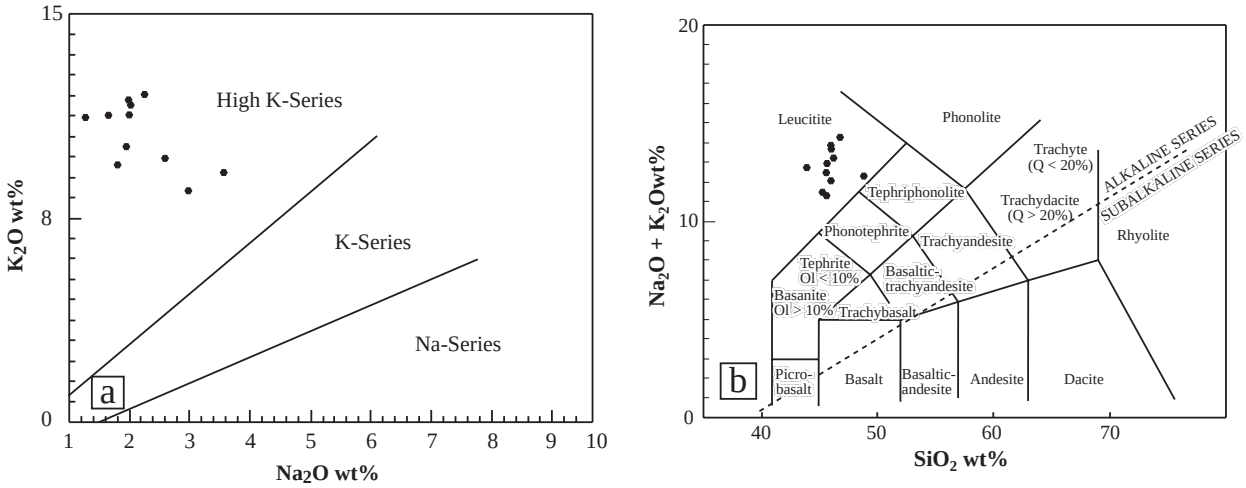

Figure 14. (a) Variation diagram of the K_2O/Na_2O vs SiO_2 for melilite leucitite; (b) Na_2O+K_2O vs SiO_2 diagram from Le Bas *et al.* (1986) for melilite leucitite. The dashed line approximates the transition between the alkaline and subalkaline series after MacDonald & Katsura (1964).

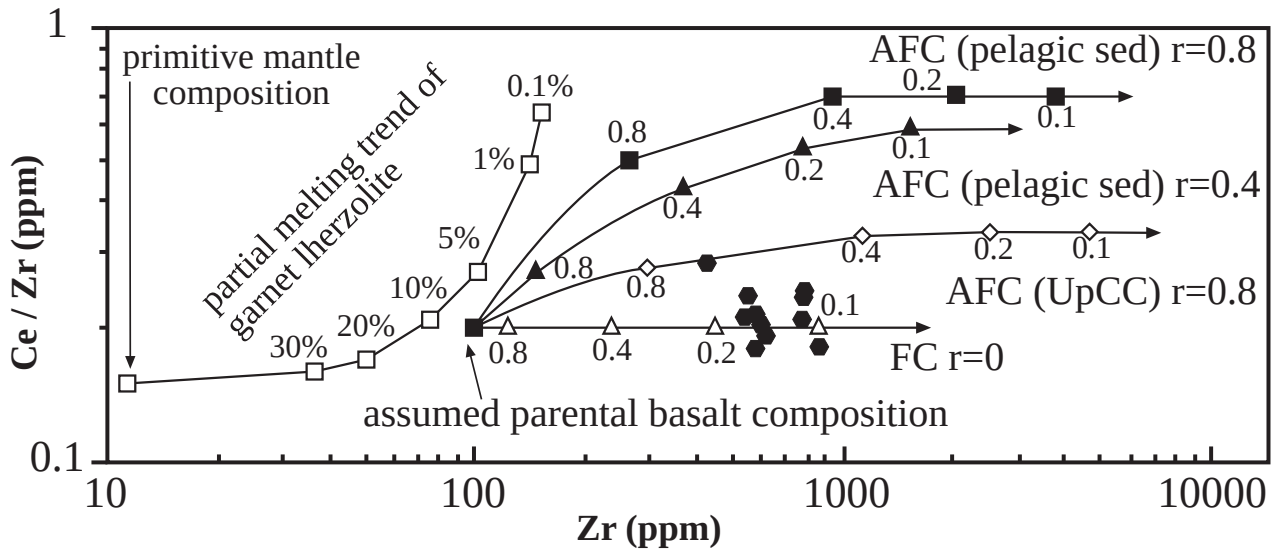

Figure 15. Modelled partial melting and assimilation with fractional crystallisation diagram of Floyd *et al.* (1996). The melilite-leucitite samples plot on the fractional-crystallisation trend of parental basalt composition. FC– fractional crystallisation, AFC– assimilation with fractional crystallisation, Up.CC– upper continental crust, r– ratio.

contamination values of the high-potassic series and non-modal melting values for garnet lherzolite. As seen from Figure 15, low Ce/Zr ratio-bearing leucitite can be generated from a primitive source by a partial-melting process (c. 10%), which is followed by fractional crystallisation.

The incompatible element characteristics of melilite leucitite samples as illustrated in Figure 16 indicate that melilite leucitites are characterised by highly fractionated patterns and strongly enrichments with respect to the normalised values of primitive mantle (Figure 16a, b). Melilite leucitites are depleted in Ba and Nb and relatively enriched in Rb, Th and Sr in chondrite-normalised diagrams of Thompson (1982) (Figure 16b). The similar trace element patterns of both sample groups suggest that melilite leucitites may be derived from same source. Rogers *et al.* (1985) indicate that enrichment processes of Ba, Nb and Ti occur in the mantle wedge above a subduction zone.

Highly fractionated REE compositions of selected representative samples of the melilite leucitite are presented in Table 6. In Figures 17 and 18, representative analyses of melilite leucitite are plotted on the C1 chondrite-normalised diagrams of Sun & McDonough (1989) and the chondrite-normalised diagram of Nakamura (1974). The REE chondrite-normalised patterns of both locations are similar, and are characterised by strong relative light rare-earth element (LREE) enrichment (Table 6). Strong enrichments of the LREE are found in many potassic volcanic rocks, from both convergent margins and continental rift zones (Bachinski & Scott 1979; Foley *et al.* 1987). This enrichment pattern suggests that lavas come from source regions, which are enriched in the LREE (Frey *et al.* 1978; Roden 1981). The patterns of two samples are almost parallel, implying that they could be related by the fractional of a phase that doesn't change the REE.

The rare-earth element compositions of some potassic volcanic rocks from Italy (Alban Hills-Roman Comagmatic Region) are given for comparison in Table 7. Alkaline potassium-rich volcanic activity in Italy occurred during the Miocene–Pleistocene (Perini *et al.* 2000) in an extensional tectonic regime. These subduction-related post-orogenic alkaline ultrapotassic rocks in Italy were products of a low degree of partial melting of a mantle peridotite enriched in incompatible elements (Peccerillo *et al.* 1984). According to Beccaluva *et al.* (1991), alkaline potassic rocks generated from mantle sources were modified by metasomatizing components, which were derived from subducted crustal materials at a destructive, post-collisional plate margin. As seen from Figure 18, the REE patterns of potassic volcanic rocks from Italy have REE patterns similar to our samples. These comparable

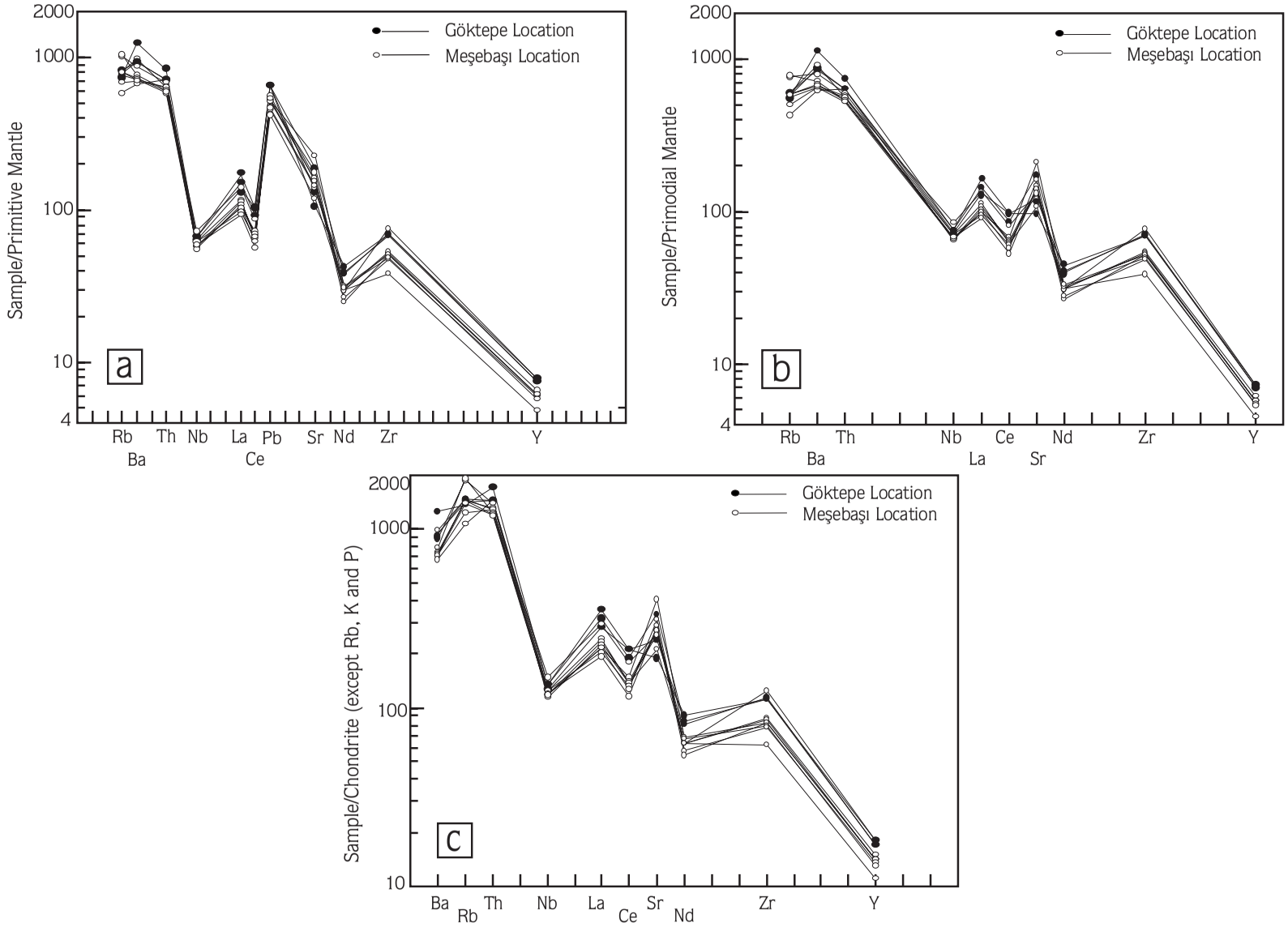

Figure 16. (a) Primitive mantle-normalised abundances of incompatible and compatible trace elements of the melilite leucitite. Normalised values are from Sun & McDonough (1989); (b) primodial mantle-normalised abundances of incompatible and compatible trace elements of melilite leucitite. Normalised values are from Wood *et al.* (1981); (c) chondrite-normalised trace element variation diagrams of melilite leucitites. Normalised values are from Thompson (1982).

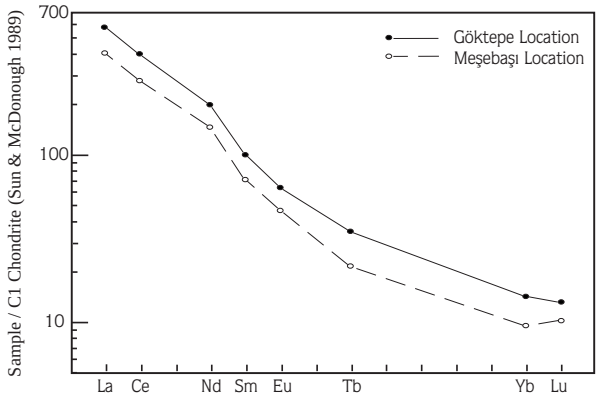

Figure 17. C1 Chondrite-normalised REE patterns for selected melilite-leucitite sample from the study area. Normalised values are from Sun & McDonough (1989).

patterns suggest that the ultrapotassic volcanic rocks of the Afyon region may have been derived from a similar source.

Foley *et al.* (1987) have subdivided the ultrapotassic ($K_2O > 3$ wt%) rocks into three subgroups based on their major-element chemistry, as follows:

Table 7. Rare-earth element contents of selected alkaline volcanic rocks from Italy.

		ITALY	
		Alban Hills-Roman Co-magmatic Region (Peccerillo 1992)	Alban Hills-Roman Co-magmatic Region (Peccerillo *et al.* 1984)
REE		HKS-MA3	Alb-2
La	(ppm)	66	111
Ce	(ppm)	133	271
Nd	(ppm)	62	-
Sm	(ppm)	125.5	21
Eu	(ppm)	2.1	4
Tb	(ppm)	0.77	2
Yb	(ppm)	2.13	2.4
Lu	(ppm)	0.33	0.45

Group I : lamproites

Group II : ultrapotassic rocks of continental rift zones

Group III : ultrapotassic rocks of active orogenic zones

As seen in Figure 19, the melilite leucitites plot in the Group III fields of the CaO vs Al_2O_3 diagram. In the CaO

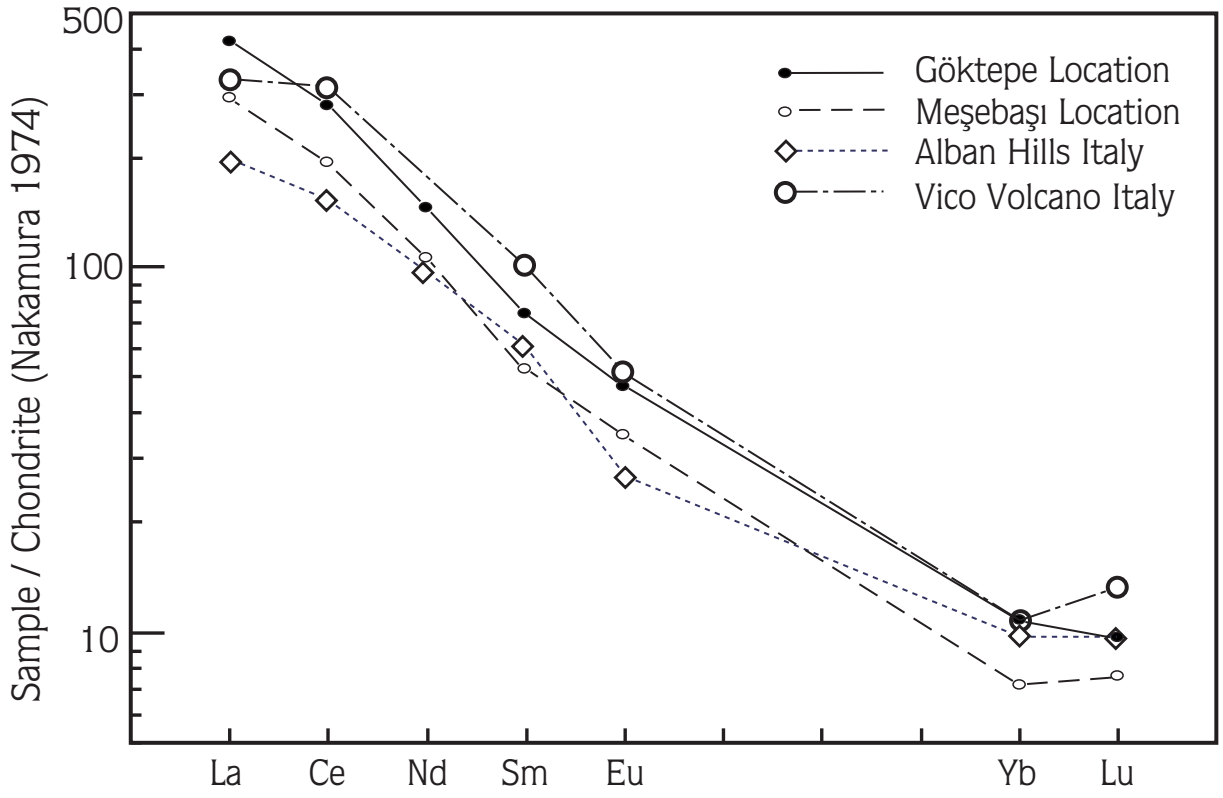

Figure 18. Chondrite-normalised REE patterns for selected melilite-leucitite samples from the study area and selected potassic volcanic rocks from Italy. Normalised values are from Nakamura (1974).

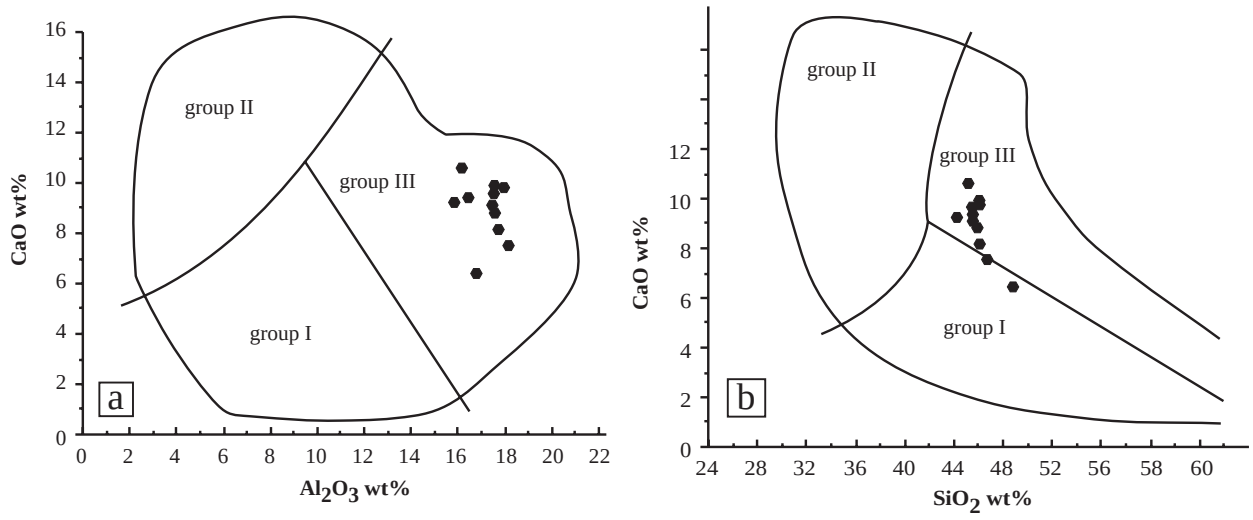

Figure 19. Classification of the Afyon volcanic rocks in the CaO versus Al_2O_3 and CaO versus SiO_2 diagrams of Foley *et al.* (1987). Group I– lamproites, Group II– ultrapotassic rocks of continental rift zones and Group III– ultrapotassic rocks of active orogenic zones.

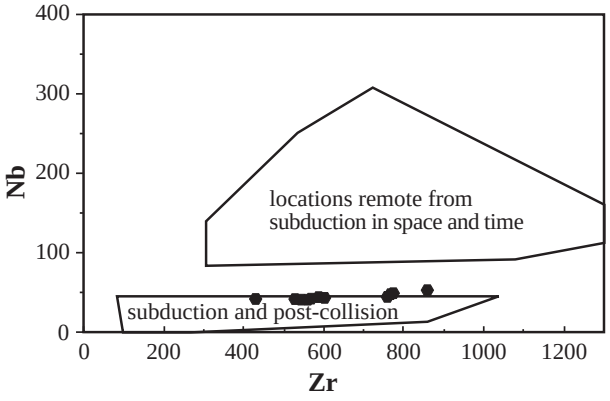

Figure 20. Variation diagram of Nb versus Zr for distinguish tectonic environments of potassic rocks (after Thompson & Fowler 1986). The Afyon samples group in the subduction/ post-collision fields.

vs SiO_2 diagrams, samples plot in the Group III field and, in two cases, in the Group I field. The Nb vs Zr variation diagram, supported by Thompson & Fowler (1986), is used for distinguishing potassic and ultrapotassic rocks related to intra-plate activity, and those authors indicated that low Nb is a characteristic feature of all subduction-related volcanic rocks. In the Nb vs Zr diagram (Figure 20), the samples plot in the subduction and post-collision fields due to their low Nb contents.

Müller *et al.* (1992) proposed tectonic discrimination diagrams for potassic volcanic rocks, based on immobile elements. On the Zr/Al_2O_3 vs TiO_2/Al_2O_3 and Y vs Zr binary diagrams, the samples are scattered on the continental arc–postcollisional-arc field (Figure 21a). On the ternary diagram, 3Zr–50Nb–Ce/P_2O_5, the samples are grouped in the postcollisional arc field (Figure 21b).

Discussion and Conclusion

Over the last 20 years, ultrapotassic lamproites have been investigated widely for their unusual mineralogical and geochemical characteristics. Foley *et al.* (1987) have suggested that potassium-rich igneous rocks should be termed "ultrapotassic" if they have high K_2O contents (>3 wt%), MgO (>3 wt%) and K_2O/Na_2O (>2 wt%) ratios. Three major chemical end-member groups were recognised by Foley *et al.* (1987) based on their major-element geochemical studies:

Group I: Lamproites

Low CaO, Al_2O_3 and Na_2O, and high K_2O/Al_2O_3 and Mg-number characterise lamproites. Incompatible elements are enriched. Mantle-derived nodules are dominated by depleted types of harzburgite and dunite.

Group II: Ultrapotassic Rocks of Continental Rift Zones

The rocks in this group have low SiO_2 and Al_2O_3 and high CaO. Incompatible elements are more depleted than in group I and there is a positive Sr spike.

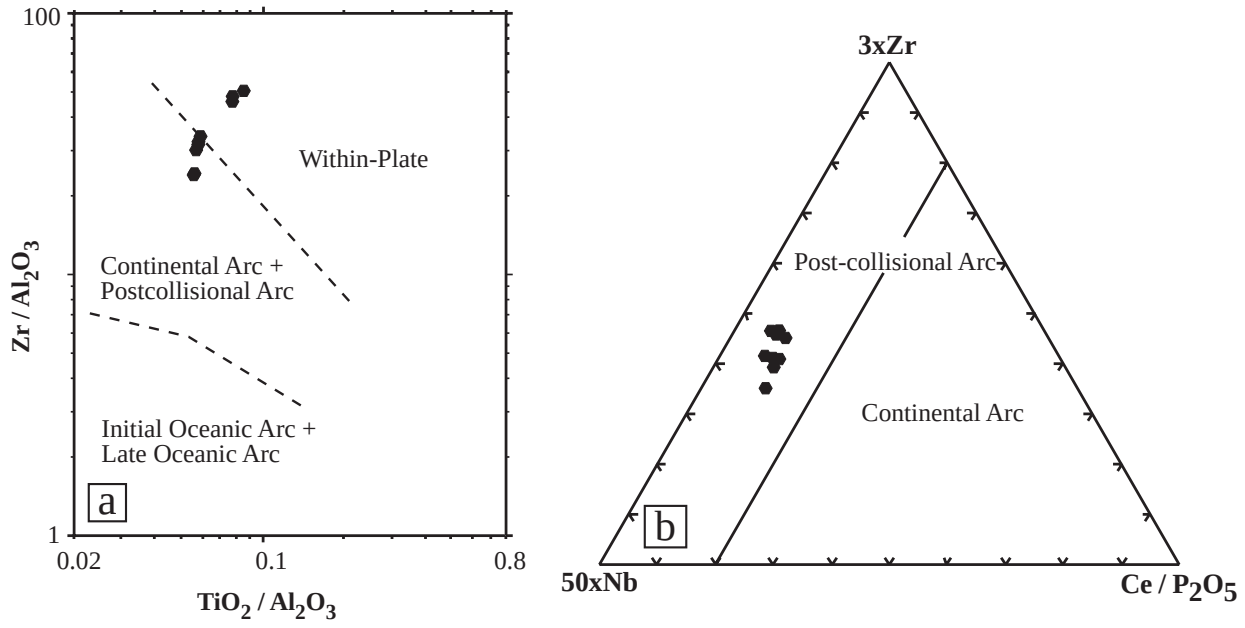

Figure 21. (a) Tectonic discrimination diagrams of Müller *et al.* (1992) for potassic volcanic rocks, based on simple ratios of immobile elements; (b) tectonic discrimination of the samples based on more exotic trace elements.

Group III: Ultrapotassic Rocks of Active Orogenic Zones

The rocks of Group III are distinguished by high Al_2O_3 and CaO. Mg-number is often low due to fractional crystallisation. The incompatible element patterns are characteristic with negative spikes for Ba, Nb, and Ti.

According to Foley *et al.* (1987), Group I rocks originate from a depleted mantle under H_2O- and F-rich, CO_2-poor and CH_4-rich conditions. The low SiO_2 and high CaO and Sr of Group II rocks suggests melting in a CO_2-rich volcanic gas. The low Ti, Nb and Ba contents of Group III rocks are explained by the presence stable titanate phases in the residue during partial melting, or reactions in the subducted slab. Foley *et al.* (1987) suggested that the high K_2O originates from subducted crustal material or from mantle metasomatism. The high CaO and Al_2O_3 are obtained via melting a fertile mantle source.

The debate about potassic suites has been focused on the relative importance of enrichment of the subcontinental mantle and crustal contamination. Most authors agree that the ultrapotassic–potassic magmas must be derived from a metasomatised or enriched mantle source (e.g., Wass & Rogers 1980; Hawkesworth *et al.* 1984; De Mulder *et al.* 1986; Rogers *et al.* 1985, 1987). Based on experimental studies, Wendlandt & Eggler (1980a, b) indicate that the parental magmas of ultrapotassic rocks were generated at different depths from a K-rich phlogopite-bearing mantle source. According to Beccaluva *et al.* (1991), the potassic-ultrapotassic magmas were generated from mantle sources modified by mantle metasomatism components derived from subducted crustal materials at a destructive, post-collisional plate margin.

The presence of ultrapotassic leucite-bearing lavas is a typical feature of Neogene to Quaternary volcanic provinces in the Mediterranean region, for example, the Roman Province of central Italy. The post-orogenic, subduction-related potassic-ultrapotassic magmatism of the Roman Province was generated from an enriched mantle source with subordinate amounts of crustal contamination. Similar examples of leucite-bearing lavas also occur in the Afyon volcanic province and the Isparta region of western Turkey.

Savaşçın *et al.* (1995) and Francalanci *et al.* (2000) indicate that ultrapotassic rocks from Afyon have primitive compositions. The lithospheric mantle source for the ultrapotassic rocks was depleted before being

metasomatised by subduction-related fluids or melts. Those authors suggested that the high Sr isotope ratios of the ultrapotassic rocks indicate that mantle metasomatism was older than the metasomatism affecting the more fertile mantle or the depleted mantle, which was metasomatised by more radiogenic subducted material.

The observed geochemical properties of ultrapotassic melilite leucitites of the study area are similar to other potassic–ultrapotassic rocks from Roman Province, Italy (Peccerillo *et al.* 1984; Beccaluva *et al.* 1991; Di Girolamo *et al.* 1991; Peccerillo 1992; Perini *et al.* 2000). Based on geochemical data, the geodynamic setting and source of the alkaline parental magma is thought to be related to widespread subduction and post-collisional processes of the Eurasian and African plates.

The undersaturated melilite-leucititic lavas of the Afyon volcanic province are highly K-rich and strongly alkaline. Na_2O/K_2O ratios are high in the melilite-leucitite samples. Melilite leucitite can be generated from a primitive source by low degrees of partial melting or from a lithospheric source previously enriched by subduction generated fluids.

Acknowledgements

Special thanks to Dr. Peter A. Floyd for his collaboration, kind help, and vital discussions throughout the studies in Department of Geology, Keele University. Thanks also to Richard Burgess for his excellent photographic work, to Peter Greatbatch and to David Wilde for thin sections, and David Emley and Margaret Aitkin for providing XRF data. Special thanks are due to Philippe D'Arco for productive discussions and his suggestion that microprobe analyses be carried out in the Universite Pierre et Marie Curie (Laboratoire de Petrologie-Mineralogique), Paris. Thanks also to Hubert Remy for organising and providing the electron-microprobe analyses. The field work was supported financially by the Dokuz Eylül University Research Foundation (Project No. 0922.95.01.05), Turkish Petroleum Corporation (TPAO), the British Council, and Franch Government. I am grateful to Cahit Helvacı for his valuable suggestions and constructive comments. Steven K. Mittwede helped with the English.

References

Aydar, E., Bayhan, H. & Zimitoğlu, O. 1996. Investigation of volcanological and petrological evolution of Afyon stratovolcano. *Yerbilimleri (Bulletin of Earth Science Application and Research Centre of Hacettepe University)* **18**, 87–107.

Bachinski, S.W. & Scott, R.B. 1979. Rare-earth and trace-element contents and the origin of minettes (mica-lamprophyres). *Geochimica et Cosmochimica Acta* **40**, 93–100.

Beccaluva, L., Di Girolamo, P. & Serri, G. 1991. Petrogenesis and tectonic setting of the Roman volcanic province, Italy. *Lithos* **26**, 191–221.

Besang, C., Eckhardt, F.-J., Harre, W., Kreuzer, H., & Müller, P. 1977. Radiometrische altersbestimmungen an neogenen eruptivgesteinen der Türkei. *Geologisches Jahrbuch Reihe* **B25**, 3–36.

Bingöl, E. 1989. *Geological Map of Turkey at 1:2,000,000 Scale*. General Directorate of Mineral Research and Exploration (MTA) Publications.

Borodin, L.S. & Pavlenko, A.S. 1974. The role of metasomatic processes in the formation of alkaline rocks. *In*: Sorensen, H. (ed), *The Alkaline Rocks.* John Wiley and Sons, New York, 515–534.

Cebria, J.M. & Lopez-Ruiz, J. 1995. Alkali basalts and leucitites in an extensional intracontinental plate setting: The Late Cenozoic Calatrava Volcanic Province (Central Spain). *Lithos* **35**, 27–46.

Clift, P. & Blusztajn, J. 1999. The trace-element characteristics of Aegean and Aeolian volcanic arc marine tephra. *Journal of Volcanology and Geothermal Research* **92**, 321–347.

Çoban, H., Yilmaz, K., Bozcu, M. & Caran, Ş. 2000. Balçıkhisar (Afyon), Senirkent (Isparta) ve Bucak (Burdur) civarında yüzeyleyen lösit içeren ultrapotasik volkanitlerin mineralojisi-petrografisi ve petrokimyası [Mineralogy-petrography and petrochemistry of leucite bearing ultrapotassic volcanics outcropping around Balçıkhisar (Afyon), Senirkent (Isparta) and Bucak (Burdur)]. *53th Geological Congress of Turkey 2000, Ankara, Abstracts,* 300–301.

Deer, W.A., Howie, R.A. & Zussman, J. 1993. *An Introduction to the Rock-Forming Minerals*. Longman, Hong Kong.

De Mulder, M. Hertogen, J., Deutsch, S. & Andre, L. 1986. The role of crustal contamination in the potassic suite of the Karisimbi Volcano (Virunga, Africa Rift Vallaey). *Chemical Geology* **57**, 117–136.

Di Girolamo, P., Melluso, L., & Morra, V. 1991. Magmatic activity northeast of Roccamonfina volcano (southern Italy): petrology, geochemistry and relationships with Campanian volcanics. *Neues Jahrbuch für Mineralogie Abhandlungen* **163**, 271–289.

Dunworth, E.A. & Wilson, M. 1998. Olivine melilites of the SW German Tertiary Volcanic Province: mineralogy and petrogenesis. *Journal of Petrology* **39**, 1905–1836.

ERCAN, T. 1979. Batı Anadolu, Trakya ve Ege adalarındaki Senozoyik volkanizması [Cenozoic volcanism in western Anatolia, Thrace, and Aegean islands]. *Bulletin of Geological Engineering* **9**, 23–46 [in Turkish with English abstract].

ERCAN, T. 1986. Orta Anadolu'daki Senozoyik volkanizması [Cenozoic volcanism in central Anatolia]. *General Directorate of Mineral Research and Exploration (MTA) Bulletin* **107**, 119–140 [in Turkish with English abstract].

ERCAN, T., GÜNAY, E. & BAŞ, H. 1983. Denizli volkanitlerinin petrolojisi ve plaka tektoniği açısından bölgesel yorumu [Petrology and plate tectonic implications of Denizli volcanics]. *Geological Society of Turkey Bulletin* **26**, 153–159 [in Turkish with English abstract].

FLOYD, P.A., WINCHESTER, J.A., CIESIELCZUK, J., LEWANDOWSKA, A., SZCZEPANSKI, J. & TURNIAK, K. 1996. Geochemistry of Early Palaeozoic amphibolites from the Orlica-Snieznik dome, Bohemian Massif: petrogenesis and palaeotectonic aspects. *Geologische Rundschau* **85**, 225–238.

FOLEY, S.F., VENTURELLI, G., GREEN, D.H. & TOSCANI, L. 1987. The ultrapotassic rocks: characteristics, classification, and constraints for petrogenetic models. *Earth-Science Reviews* **24**, 81–134.

FRANCALANCI, L., CIVETTA, L., INNOCENTI, F. & MANETTI, P. 1990. Tertiary–Quaternary alkaline magmatism of the Aegean-western Anatolian area: a petrological study in the light of new geochemical and isotopic data. *In*: SAVAŞCIN, M.Y. & ERONAT, A.H. (eds), *International Earth Science Colloquium on the Aegean Region (IESCA) Proceedings* **II**, 385–396.

FRANCALANCI, L., INNOCENTI, F., MANETTI, P. & SAVAŞCIN, Y. 2000. Neogene alkaline volcanism of the Afyon-Isparta area, Turkey: petrogenesis and geodynamic implications. *Mineralogy and Petrology* **70**, 285–312.

FREY, F.A., GREEN, D.H. & ROY, S. 1978. Integrated models of basalt petrogenesis: a study of quartz tholeiites to olivine melilitites from SE Australia utilizing geochemical and experimental petrological data. *Journal of Petrology* **19**, 463–579.

FYTIKAS, M., INNOCENTI, F., MANETTI, P., MAZZUOLI, R., PECCERILLO, A., & VILLARI, L. 1984. Tertiary to Quaternary evolution of volcanism in the Aegean region. *In*: DIXON, J.E. & ROBERTSON, A.H.F. (eds), *The Geological Evolution of the Eastern Mediterranean*. Geological Society, London, Special Publications **17**, 687–699.

HAWKESWORTH, C.J., ROGERS, N.W., VAN CALSTEREN, P.W.C. & MENZIES, M.A. 1984. Mantle enrichment processes. *Nature* **311**, 331–335.

INNOCENTI, F., KOLIOS, N., MANETTI, P., RITE, F. & VILLARI, L. 1982. Acid and basic Late Neogene volcanism in central Aegean Sea: its nature and geotectonic significance. *Bulletin of Volcanology* **45**, 87–97.

JUNG, S. 1995. Geochemistry and petrogenesis of rift-related Tertiary alkaline rocks from the Rhön area (central Germany). *Neues Jahrbuch für Mineralogie Abhandlungen* **169**, 193–226.

KAYA, O. 1981. Miocene reference section for the coastal parts of western Anatolia. *Newsletter for Stratigraphy* **10**, 164–191.

KAYA, O. 1982. Petrologic significance of the Miocene volcanic rocks in Menemen, western Anatolia. *Aegean Earth Science* **1**, 45–58.

KELLER, J. 1983. Potassic lavas in the orogenic volcanism of the Mediterranean area. *Journal of Volcanology and Geothermal Research* **18**, 321–335.

KELLER, J. & VILLARI, L. 1972. Rhyolitic ignimbrites in the region of Afyon (central Anatolia). *Bulletin Volcanologique* **36**, 342–358.

KOÇYİĞİT, A. 1984. Güneybatı Türkiye ve yakın dolayında levhaiçi yeni tektonik gelişim [Intra-plate neotectonic development in southwestern Turkey and adjacent areas]. *Geological Society of Turkey Bulletin* **27**, 1–16 [in Turkish with English abstract].

LE BAS, M.J., LE MAITRE, R.W., STRECKEISEN, A. & ZANETTIN, B. 1986. A chemical classification of volcanic rocks based on the total alkali-silica diagram. *Journal of Petrology* **27**, 745–750.

MACDONALD, G.A. & KATSURA, T. 1964. Chemical composition of Hawaiian lavas. *Journal of Petrology* **5**, 82–133.

MARIMOTO, N. 1989. Nomenclature of pyroxenes. *Canadian Mineralogist* **27**, 143–156.

MÜLLER, D., ROCK, N.M.S. & GROVES, D.I. 1992. Geochemical discrimination between shoshonitic and potassic volcanic rocks in different tectonic settings: a pilot study. *Mineralogy and Petrology* **46**, 259–289.

NAKAMURA, N. 1974. Determination of REE, Ba, Fe, Mg, Na, and K in carbonaceous and ordinary chondrites. *Geochimica et Cosmochimica Acta* **38**, 757–773.

NEUBAUER, F. & RAUMER, J.V. 1993. The Alpine basement-linkage between Variscides and east-Mediterranean mountain belt. *In*: RAUMER, J.F. & NEUBAUER, F. (eds), *Pre Mesozoic Geology in the Alps*. Springer-Verlag, 641–664.

ÖZGENÇ, İ. 1993. Kızılcaören (Sivrihisar-Eskişehir) karbotermal bastneazit-fluorit-barit yatağının jeolojisi ve nadir toprak element jeokimyası [Geology and rare-earth element geochemistry of carbothermal bastnaesite-fluorite-barite deposit of Kızılcaören (Sivrihisar–Eskişehir)]. *Geological Society of Turkey Bulletın* **36**, 1–11 [in Turkish with English abstract].

ÖZGÜL, N. 1984. Stratigraphy and tectonic evolution of the central Taurides. *In*: TEKELİ, O. & GÖNCÜOĞLU, M.C. (eds), *Geology of the Taurus Belt.* Proceedings of the International Tauride Symposium. General Directorate of Mineral Research and Exploration Institute (MTA) Publications, 77–90.

ÖZTÜRK, E.M. & ÖZTÜRK, Z. 1989. *Balçıkhisar–Karadilli (Afyon)–Dereköy (Isparta) Dolayının Jeolojisi: Göller Bölgesi Projesi [The Geology Around Balçıkhisar–Karadilli (Afyon)–Dereköy (Isparta)*: *The Lakes District Project]*. General Directorate of Mineral Research and Exploration (MTA), Report no: IV/01.0.01.08.14, [in Turkish, unpublished].

PASQUARE, S., POLI, S., VEZZOLI, L. & ZANCHI, A. 1988. Continental arc volcanism and tectonic setting in central Anatolia, Turkey. *Tectonophyics* **146**, 217–230.

PECCERILLO, A. 1992. Potassic and ultrapotassic rock: compositional characteristics, petrogenesis, and geological significance. *Episodes* **15**, 243–251.

PECCERILLO, A., POLI, G. & TOLOMEO, L. 1984. Genesis, evolution and tectonic significance of K-rich volcanics from the Alban Hills (Roman comagmatic region) as inferred from trace-element geochemistry. *Contributions to Mineralogy Petrology* **86**, 230–240.

PERINI, G., CONTICELLI, S., FRANCALANCI, L. & DAVIDSON, J.P. 2000. The relationship between potassic and calc-alkaline post-orogenic magmatism at Vico volcano, central Italy. *Journal of Volcanology and Geothermal Research* **95**, 247–272.

POISSON, A., AKAY. E., DUMONT, J.F. & UYSAL, Ş. 1984. The Isparta Angle: a Mesozoic paleorift in the western Taurides. *In*: TEKELİ O. & GÖNCÜOĞLU, M.C. (eds), *Geology of the Taurus Belt*. Proceedings of the International Tauride Symposium. General Directorate of Mineral Research and Exploration Institute (MTA) Publications, 11–26.

ROGERS, N.W., PARKER, R.J., HAWKESWORTH, R.J. & MARSH, J.S. 1985. The geochemistry of potassic lavas from Vulsini, Central Italy, and implications for mantle enrichment process beneath the Roman region. *Contributions to Mineralogy Petrology* **90**, 244–257.

ROGERS, N.W., HAWKESWORTH, C.J., MATTEY, D.P. & HARMON, R.S. 1987. Sediment subduction and the source of potassium in orogenic leucitites. *Geology* **15**, 451–453.

RODEN, M.F. 1981. Origin of coexisting minette and ultramafic breccia, Navajo Volcanic Field. *Contributions to Mineralogy Petrology* **11**, 195–206.

SAHAMA, TH.G. 1968. Mineralogical composition of the Nyiragongo rocks. *Geologische Rundschau* **57**, 904–914.

SAHAMA, TH.G. & MEYER, A. 1958. *Study of the Volcano Nyiragongo.* A Progress Report. Exploration du pare national Albert, mission d'Etudes vulcanologiques, number 2.

SAVAŞÇIN, M.Y. 1990. Magmatic activities of Cenozoic compressional and extensional tectonic regime in western Anatolia. *In*: SAVASÇIN, M.Y., & ERONAT, A.H. (eds), *International Earth Science Colloquium on the Aegean Region (IESCA) Proceedings* II, 420–434.

SAVAŞÇIN, M.Y. & GÜLEÇ, N. 1990. Relations between magmatic and tectonic activities in western Turkey. Geological and geochemical features with examples from the coastal section. *In*: SAVAŞÇIN, M.Y. & ERONAT, A.H. (eds), *International Earth Science Colloquium on the Aegean Region (IESCA) Proceedings* II, 300–313.

SAVASÇIN, M.Y., FRANCALANCI, L., INNOCENTI, F., MANETTI, P., BIRSOY, R. & DAĞ, N. 1995. Miocene-Pliocene potassic ultrapotassic volcanism of the Afyon-Isparta region (central-western Anatolia-Turkey): petrogenesis and geodynamic implication. *In*: PIŞKİN, Ö., ERGÜN, M., SAVASÇIN, M.Y. & TARCAN, G. (eds), *International Earth Science Colloquium on the Aegean Region (IESCA) Proceedings* II, 487–502.

SUN, S.S. & MCDONOUGH, W.F. 1989. Chemical and isotope systematics of ocean basalts: implications for mantle composition and processes. *In*: SAUNDERS, A.D. & NORRY, M.J. (eds), *Magmatism in the Ocean Basins*. Geological Society, London, Special Publications **42**, 313–345.

THOMPSON, R.N. 1982. Magmatism of the British Tertiary Volcanic Province. *Scottish Journal of Geology* **18**, 49–107.

THOMPSON, R.N. & FOWLER, M.B. 1986. Subduction-related shoshonitic and ultrapotassic magmatism: a study of Siluro-Ordovician syenites from the Scottish Caledonides. *Contributions to Mineralogy Petrology* **94**, 507–522.

TOSCANI, L., CAPEDRI, S. & ODDONE, M. 1990. New chemical and petrographic data of some undersaturated lavas from Nyiragongo and Mikeno (Virunga-Western Africa Rift-Zaire). *Neues Jahrbuch für Mineralogie Abhandlungen* **161**, 287–302.

VELDE, D. & YODER, H.S.JR, 1977. Melillite and melilite-bearing igneous rocks. *Carnegie Institution of Washington, Year Book* **76**, 478–485.

WASS, S.Y. & ROGERS, N.W. 1980. Mantle metasomatism-precursor to continental alkaline volcanism. *Geochimica et Cosmochimica Acta* **44**, 1811–1823.

WENDLANDT, R.F. & EGGLER, D.H. 1980a. The origin of potassic magmas: 1. melting relations in the systems $KAlSiO_4$-Mg_2SiO_4-SiO_2 and $KalSiO_4$-MgO-SiO_2-CO_2 to 30 kilobars. *American Journal of Science* **280**, 385–420.

WENDLANDT, R.F. & EGGLER, D.H. 1980b. The origin of potassic magmas: 2. Stability of phlogopite in natural spinel lherzolite and in the system $KalSiO_4$-MgO-SiO_2-H_2O-CO_2. *American Journal of Science* **208**, 421–458.

WOOD, D.A., TARNEY, J. & WEAVER, B.L. 1981. Trace element variations in Atlantic Ocean basalts and Proterozoic dykes from northwest Scotland: their bearing upon the nature and geochemical evolution of the upper mantle. *Tectonophysics* **75**, 91–112.

YILMAZ, Y. 1989. An approach to the origin of young volcanic rocks of western Turkey. *In*: ŞENGÖR, A.M.C. (ed), *Tectonic Evolution of the Tethyan Region*. Dordrecht-Netherlands-Kluwer Academic Publishers, 159–189.

Received 24 July 2002; revised typescript accepted 23 October 2003